Scalable computation for Bayesian hierarchical models

Omiros Papaspiliopoulos Tim Stumpf-Fetizon
Giacomo Zanella

March 1, 2025

The article is about algorithms for learning Bayesian hierarchical models, the computational complexity of which scales linearly with the number of observations and the number of parameters in the model. It focuses on crossed random effect and nested multilevel models, which are used ubiquitously in applied sciences, and illustrates the methodology on two challenging real data analyses on predicting electoral results and real estate prices respectively. The posterior dependence in both classes is sparse: in crossed random effects models it resembles a random graph, whereas in nested multilevel models it is tree-structured. For each class we develop a framework for scalable computation based on collapsed Gibbs sampling and belief propagation respectively. We provide a number of negative (for crossed) and positive (for nested) results for the scalability (or lack thereof) of methods based on sparse linear algebra, which are relevant also to Laplace approximation methods for such models. Our numerical experiments compare with off-the-shelf variational approximations and Hamiltonian Monte Carlo. Our theoretical results, although partial, are useful in suggesting interesting methodologies and lead to conclusions that our numerics suggest to hold well beyond the scope of the underlying assumptions.

Keywords: Gibbs sampler, sparse linear algebra, belief propagation, random graphs, crossed random effects, multilevel models, electoral surveys

1. Motivation and a taster of the results

1.1. Scalable Bayesian computation

In this article we explore - methodologically, mathematically and computationally - efficient computational frameworks for Bayesian learning in large scale hierarchical models.

We focus on two canonical hierarchical structures, which are arguably the two most common in applied Statistics; nested multilevel models, introduced in Section 1.3 below, where data is organized in hierarchical clusters and parameters in a given level in the hierarchy are shrunk to (fewer) parameters in the deeper level; and crossed effect models, introduced in Section 1.2, where the data is organized in a multidimensional contingency table and the within-cell distribution is modelled in terms of a linear expansion of a priori independent effects. Both models involve a potentially high-dimensional vector of regression parameters, denoted generically by $\boldsymbol{\theta}$ in this paper, and a low-dimensional vector of variance parameters that control the shrinkage on the regression parameters, which are denoted generically by $\boldsymbol{\gamma}$. The vector of available data will be denoted generically by $\boldsymbol{y}$. All the models we consider will have additional covariates but we will suppress them from the notation and "data" will refer to available response observations $\boldsymbol{y}$. The total number of observations $\boldsymbol{y}$ will be denoted by N and that of the total number of regression parameters $\boldsymbol{\theta}$ will be denoted by p. In terms of notation, throughout the article bold face letters denote vectors (when lowercase) and matrices (when upper case).

The computational challenge is to obtain samples from the posterior distribution $\mathcal{L}(\boldsymbol{\theta}, \gamma \mid \boldsymbol{y})$, where $\mathcal{L}(\cdot \mid \cdot)$ will be used in the article to refer to conditional distributions. The "holy grail" is algorithms whose *complexity* scales linearly in N and p, and we call such algorithms *scalable*. The complexity of MCMC sampling algorithms is the product of cost per iteration and the number of iterations required (see Section 3.2). We are interested in high-dimensional asymptotic regimes where both N and p are large, even if most complexity theory we develop in this paper is non-asymptotic.

The theoretical and methodological work in this article is motivated by, and illustrated on, two consulting-type applications the authors have been involved with. These are described below together with a generic description of the models our work is relevant for, a first numerical illustration of what can be achieved with the methods we propose, and a glimpse into the theory we develop in this work.

1.2. Crossed effect models and predicting electoral outcomes

Crossed effect models are the canonical framework for modelling the dependence of an output variable on a number of categorical input variables. In the literature they appear under various names, e.g. cross-classified data, variance component models or multi-way analysis of variance (Gelman, 2005; Searle et al., 2009; Volfovsky and Hoff, 2014).

A simple example, which can be thought of as a basic (effectively, rank-one) model for recommendation, is the two-factor crossed effect model:

$$\mathcal{L}(y_{ij} \mid \boldsymbol{a}) = \mathcal{N}(a^{(0)} + a_i^{(1)} + a_j^{(2)}, (n_{ij}\tau)^{-1}), \quad i = 1, \dots, I_1, \quad j = 1, \dots, I_2,$$

where it is convenient to think of i as indexing a customer (or a customer type), j a product and y_{ij} as a product rating (or an average of such ratings among all customers of this type). Here $n_{ij} = 0$ if the product has not been rated, $a^{(0)}$ is a global mean, $a_i^{(1)}$ are customer latent effects and $a_j^{(2)}$ are product latent effects. The latent variables are modelled via exchangeable Gaussian distributions, $a_\ell^{(k)} \sim \mathcal{N}(0, 1/\tau_k)$, and $a^{(0)}$ is given an improper flat prior. Using such ingredients one can build models for recommendation, e.g. Perry (2016), although in this article we simply use the connection to build intuition on certain data designs and assumptions we employ in our complexity analysis. For example, an interesting high-dimensional regime consistent with practical applications is one where only a small fraction of the customer-product combinations is observed, i.e., where the number of observations N satisfies $N \ll I_1 \times I_2$, see (Gao and Owen, 2017) for discussion.

A general K-factor crossed effect model is obtained as follows. There are K categorical input variables, known as factors, each with I_k categories, known as levels. Each combination of levels of the different factors defines a cell in a contingency table. The observations at each cell, if any, can be in principle multivariate, as in the electoral survey motivating application we have below; let L denote the observation dimension. Where appropriate, we denote by $\boldsymbol{X}_j$ the covariates associated to the j-th observation, excluding the intercept, and by $\boldsymbol{\beta}$ the associated linear regression coefficients. Then, in this generality the crossed effect model is as follows:

$$\begin{aligned}
\mathcal{L}(\boldsymbol{a}^{(0)}) &= \mathcal{N}(\boldsymbol{\mu}_{pr}, \boldsymbol{T}_{pr}^{-1}),\\
\mathcal{L}(\boldsymbol{a}^{(k)} \mid \boldsymbol{T}_k) &= \mathcal{N}(\boldsymbol{0}, (\boldsymbol{T}_k \otimes \boldsymbol{I})^{-1}), \quad k = 1, \dots, K\\
\mathcal{L}(\boldsymbol{y}_j \mid \boldsymbol{a}, \boldsymbol{\beta}) &= \mathcal{L}(\boldsymbol{y}_j \mid \boldsymbol{\eta}_j)\\
\boldsymbol{\eta}_j &= \boldsymbol{X}_j\boldsymbol{\beta} + \boldsymbol{a}^{(0)} + \boldsymbol{a}^{(1)}_{i_1[j]} + \cdots + \boldsymbol{a}^{(K)}_{i_K[j]}, \quad j = 1, \dots, N.
\end{aligned} \tag{1}$$

Above, $\otimes$ stands for the Kronecker product, $\boldsymbol{T}_k$ are $L \times L$ precision matrices modelling the dependence among the elements of $\boldsymbol{a}^{(k)}_{i_k}$, $\boldsymbol{a}^{(k)}$ is the vector of all stacked $\boldsymbol{a}^{(k)}_{i_k}$'s, $\boldsymbol{I}$ are identity matrices of appropriate dimensions, and $i_k[j]$ denotes the level of the k-th category associated to the j-th observation (see, e.g., Section 1.1 and Chapter 11 of Gelman and Hill (2007) for this type of notation). The fixed effects coefficients $\boldsymbol{\beta}$ are typically assigned a normal or a flat prior. There might be further unknown (typically precision) parameters at the data level, as e.g., in the Gaussian model in (1.2), and we will be explicit in special cases. In our numerical illustrations we focus on two special cases: Gaussian models, where $\mathcal{L}(\boldsymbol{y}_j \mid \boldsymbol{\eta}_j) = \mathcal{N}(\boldsymbol{\eta}_j, \tau^{-1}\boldsymbol{I})$, and multinomial logistic models where $\boldsymbol{y}_j \mid \boldsymbol{\eta}_j \sim \mathit{Categorical}(\text{softmax}\{\boldsymbol{\eta}_j\})$,

$$\text{softmax}\{\boldsymbol{\eta}\} = \left(\frac{e^{\eta_1}}{\sum_\ell e^{\eta_\ell}}, \cdots, \frac{e^{\eta_L}}{\sum_\ell e^{\eta_\ell}}\right), \tag{2}$$

and $\boldsymbol{y}_j$ is an L-dimensional vector of all zeros and a single one (one-hot encoding).

For computational convenience, we adopt conjugate priors for the prior precision matrices $\boldsymbol{T}_k$. In the most general setting where $\boldsymbol{T}_k$ is a full rank matrix,

$$\mathcal{L}(\boldsymbol{T}_k) = \mathcal{W}(\nu_k, \boldsymbol{I}/\nu_k) \tag{3}$$

a priori. The multinomial logit model introduces the further complication of being ill-identified due to softmax being invariant under translations of $\boldsymbol{\eta}$. Thus, we follow the common practice of introducing an identifiability constraint, although our methods work with alternative formulations as well.

k	factor name	no. of levels (I_k)
1	`province id`	52
2	`activity`	4
3	`age`	3
4	`education`	3
5	`municipality size`	3
6	`last vote`	3
7	`gender`	2
-	response	3

Table 1.: Categorical factors included in the crossed effects application.

Electoral surveys, consisting of the self-reported voting intention and various demographic traits for a sample of potential voters, provide one of the most natural applications for crossed-effects modeling. Here the response variable is the multi-categorical voting intention, with each category corresponding to a different party. Demographic traits such as location and age serve as input variables; these may be stratified into multi-categorical variables. From a forecasting perspective, the main benefit of modeling the relationship of voting intention and demographic traits is that it enables *post-stratification*, where we combine the model with exact knowledge of the frequency of the demographic traits, obtained for example from a census. Compared to predicting the election result according to the raw voting intention counts of the survey, post-stratification typically reduces both the bias and the variance of the forecast. As our concrete example, we pick the pre-electoral survey carried out by the *Centro de Investigaciones Sociológicas* (CIS) ahead of the November 2019 Spanish general elections. In contrast with the more commonly considered 2-party system in the US, the Spanish system has recently fragmented into 5 nationally competitive parties.

Such electoral surveys are useful both for disaggregating the national voting intention to local districts, which is crucial for predicting parliamentary representation, and for dealing with insurgent political parties with significant electoral success, which is becoming a common phenomenon in European politics. On the other hand, such surveys are few and do not capture the electoral sentiment near the election time. Hence, it is interesting to synthesize them with national polls carried out by media outlets and institutions. Montalvo et al. (2019) propose such a Bayesian evidence synthesis framework, a component of which is the electoral survey crossed effect model, which we focus upon here. For the analysis in this paper we focus on a simplified data structure with $L = 3$ parties, $K = 7$ input variables, and $p = 140$ regression parameters overall (due to the identifiability constraint there are 2 per level, and $I = 70$ levels overall). The $N = 9234$ survey respondents may be sorted according to the input variables into a table with $I_1 \times \cdots \times I_K = 33696$ cells. Of these cells, only 4764 contain any respondents; the table is, in that specific sense, *sparse*. Table 1 summarises the dataset characteristics.

Here is an illustration of the computational advantages of the methodology we develop in this article. Section 3.1 proposes a collapsed Gibbs sampling methodology for sampling the posterior of parameters in models (1). Figure 1 compares the approximation of posterior means and posterior standard deviation of the regression parameters in this model for the electoral survey dataset, as produced by our proposed scheme and by a mean field variational Bayes inference as implemented in *Stan*. Section 6 contains details of the experiment, but an interesting finding can already be appreciated. For the same amount of available computational time, our proposed MCMC method provides more accurate estimates than the off-the-shelf variational inference approximation, challenging the widely accepted perception that the latter is fast and less accurate and the former is slow but more accurate: here MCMC is fast and accurate.

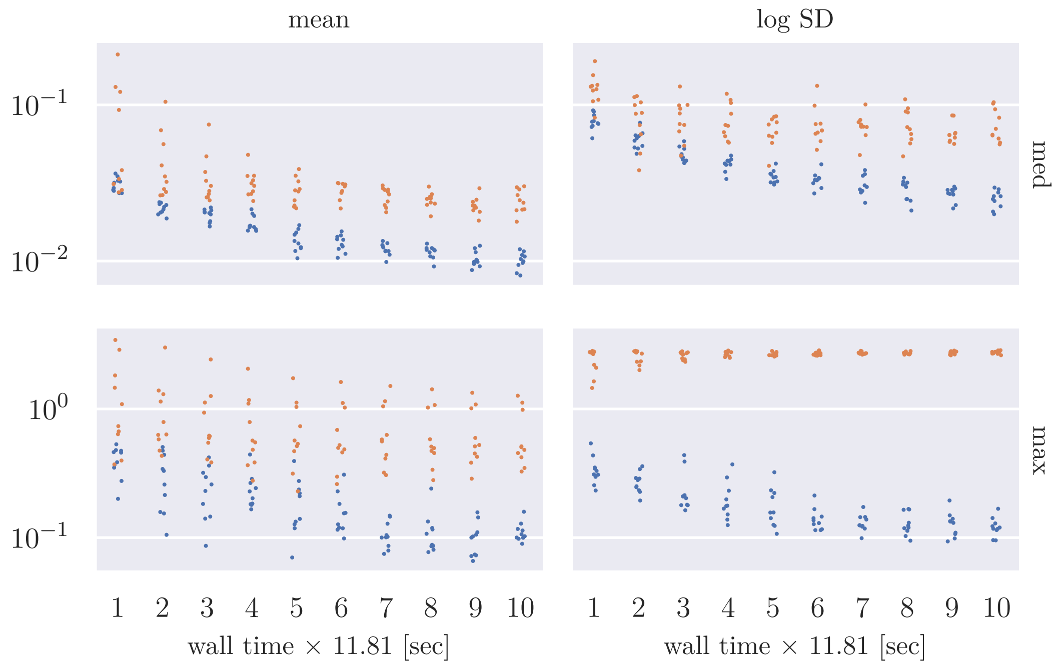

Figure 1.: *(Crossed effects elections model)* Comparison of estimation accuracy between the collapsed Gibbs sampler (blue) and Stan/ADVI (orange). The panels show absolute error in estimating posterior mean and log posterior standard deviation of the model coefficients ($\boldsymbol{\theta}$) as a function of run time. Each dot refers to a single run of the algorithm (there are 10 runs overall). Results are horizontally split by posterior summary and vertically by error quantile (median or max across all regression coefficients). More details on the numerics available in Section 6.

Section 3.2 proves that the proposed MCMC algorithm for models (1) under certain assumptions is *scalable*. Rewardingly, to a good extent the theoretical analysis has motivated the methodology in this context, not the other way round. The posterior dependence structure among the regression parameters in crossed-effect models for typical applications is *sparse*, and this is a key component of the success of the proposed collapsed Gibbs sampler. However, this is a subtle point: Section 4.4 proves that under the same assumptions for which the collapsed Gibbs sampler is scalable, approaches based on sparse linear algebra are not.

1.3. Nested multilevel models and real estate price prediction

Nested multilevel models (Gelman and Hill, 2007) is the basic hierarchical structure for data and parameters naturally organized into nested clusters. A simple example is the two-level hierarchical model

$$\begin{aligned} \mathcal{L}(\boldsymbol{\beta}_0) &= \mathcal{N}(\boldsymbol{\mu}_{pr}, \boldsymbol{T}_{pr}^{-1}) \\ \mathcal{L}(\boldsymbol{\beta}_i \mid \boldsymbol{\beta}_0) &= \mathcal{N}(\boldsymbol{\beta}_0, \boldsymbol{\Sigma}_0) \\ \mathcal{L}(\boldsymbol{y}_i \mid \boldsymbol{\beta}_i) &= \mathcal{N}(\boldsymbol{X}_i\boldsymbol{\beta}_i, \tau_1^{-1}\boldsymbol{I}). \end{aligned} \tag{4}$$

where we understand the limiting case $\boldsymbol{\mu}_{pr} = \mathbf{0}, \boldsymbol{T}_{pr} = \mathbf{0}\mathbf{0}^T$ as the improper flat prior on $\boldsymbol{\beta}_0$. The level furthest from the data will be understood as the deepest. According to this model, at the data level there is a regression model, one for each data cluster i; the amount of observations, $dim(\boldsymbol{y}_i)$, will typically vary with i; the regression coefficients $\boldsymbol{\beta}_i$ are shrunk towards a common value $\boldsymbol{\beta}_0$, which is modelled either by a Gaussian with known hyperparameters, or by an improper prior at the deepest level. We opt for a formulation that permits rank-deficient covariance matrices at deeper levels, e.g., $\boldsymbol{\Sigma}_0$ above, which allows us to fit in this framework mixed-effects models as discussed for example in Gelman and Hill (2007, Section 13.3).

A quite general definition of a nested multilevel hierarchical model is as follows, which allows for covariates and data at all levels of the hierarchy and patterns of missing data:

$$\begin{aligned} \mathcal{L}(\boldsymbol{\beta}_0) &= \mathcal{N}(\boldsymbol{\mu}_{pr}, \boldsymbol{T}_{pr}^{-1}) \\ \mathcal{L}(\boldsymbol{\beta}_{i_1\ldots i_k} \mid \boldsymbol{\beta}_{i_1\ldots i_{k-1}}) &= \mathcal{N}(\boldsymbol{A}_{i_1\ldots i_k}\boldsymbol{\beta}_{i_1\ldots i_{k-1}}, \boldsymbol{\Sigma}_{i_1\ldots i_{k-1}}), \quad k = 1, \ldots, K \\ \mathcal{L}(\boldsymbol{y}_{i_1\ldots i_k} \mid \cdot) &= \mathcal{L}(\boldsymbol{y}_{i_1\ldots i_k} \mid \boldsymbol{\eta}_{i_1\ldots i_k}), \quad \boldsymbol{\eta}_{i_1\ldots i_k} = \boldsymbol{X}_{i_1\ldots i_k}\boldsymbol{\beta}_{i_1\ldots i_k}. \end{aligned} \tag{5}$$

The dimension of the regression parameters at each leaf of the tree will be denoted by L. The $\boldsymbol{X}_{i_1\ldots i_k}$'s and the $\boldsymbol{A}_{i_1\ldots i_k}$'s are matrices of covariates and design parameters. In the simplest but also most common situation we might have data only at the highest level K, but there are interesting situations where data are available at different depths. The last line defines that conditionally on the whole set of regression parameters, the distribution of the data $\boldsymbol{y}_{i_1\ldots i_k}$ on a leaf depends only on the linear predictor $\boldsymbol{\eta}_{i_1\ldots i_k}$. In many applications, including the one that motivates our work and is described below, in Section 6, the covariance matrices are level-dependent and not leaf-dependent, hence take $\mathcal{L}(\boldsymbol{\beta}_{i_1\ldots i_k} \mid \boldsymbol{\beta}_{i_1\ldots i_{k-1}}) = \mathcal{N}(\boldsymbol{A}_{i_1\ldots i_k}\boldsymbol{\beta}_{i_1\ldots i_{k-1}}, \boldsymbol{\Sigma}_{k-1})$. In the case of Gaussian likelihood we set $\mathcal{L}(\boldsymbol{y}_{i_1\ldots i_k} \mid \boldsymbol{\eta}_{i_1\ldots i_k}) = \mathcal{N}(\boldsymbol{\eta}_{i_1\ldots i_k}, \tau_{i_1\ldots i_k}^{-1}\boldsymbol{I})$ and set formally $\tau_{i_1\ldots i_k} = 0$ when data are unavailable at a given location in the hierarchy. The methodology we develop can be extended to non-Gaussian likelihoods, and we discuss some possibilities in Section 7. We set conjugate Inverse-Wishart priors for all unknown covariance matrices, where appropriate.

We have explored this framework in a project on temporal prediction of real estate prices at high spatial resolution. Our approach synthesizes a type of multilevel capital asset pricing model, which we describe below, that relates the local average square meter price of different type of real estate properties to national economic price indices, such as GDP, with a multivariate time series model for these indices. In this article we focus on the multilevel regression component of this agenda. Due to confidentiality constraints, we work with a dataset that has been simulated from a misspecified version of (5) using the part of the dataset that is publicly available and parameter values that are consistent with the real data.

In our application the spatial domain is Spain organized according to 5-digit postal codes, which define $K = 4$ levels plus the root, since the first two digits define a province in the country and the later codes correspond to higher spatial resolutions. There are 44 observations at each postal code, each of which is the differences in consecutive quarters of the logarithm of local average sales price. The quarters span the period 2007-2018. The predictors are available only at the leaf-level and are an intercept and a national housing price index, hence $L = 2$. In this data structure, there are $p \approx 8 \times 10^3$ regression parameters and $N \approx 4 \times 10^6$ observations.

Section 4.3 establishes that methods based on sparse linear algebra methods are *scalable* for nested multilevel models and Section 5.3 connects them to belief propagation. Figure 2 compares the efficiency of the MCMC scheme based on sparse linear algebra to that of the NUTS implementation of Hamiltonian Monte Carlo as delivered in *Stan*. Sec-

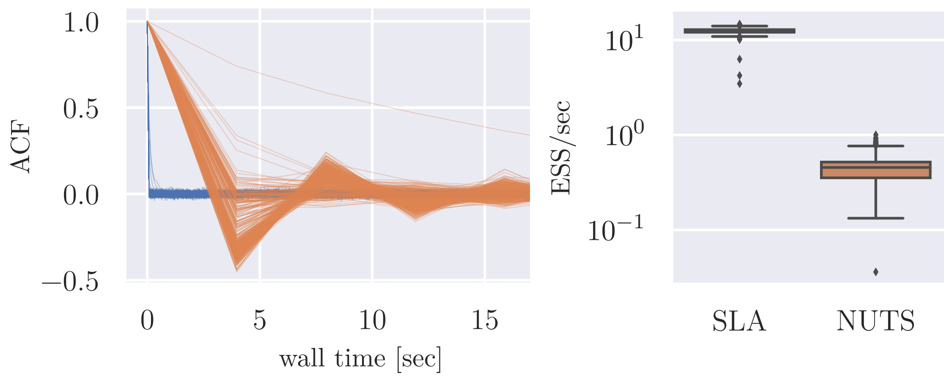

Figure 2.: *(Nested effects real estate model)* Comparison of sampling efficiency MCMC based on sparse linear algebra and Stan/NUTS (orange). The left panel overlays ACFs of $\boldsymbol{\theta}$ and $\boldsymbol{\gamma}$ as a function of wall time. The right panel shows the distribution of effective samples per second. Due to the large number of parameters, we only plot ACFs for a subset. For each algorithm, we include ACFs for the 20 slowest parameters and a representative subsample of the rest. More details on the numerics available in Section 6.

tion 6 provides detailed comparisons, but it can already be appreciated the huge speeds ups that are possible in nested multilevel models by exploiting sparse linear algebra or equivalently belief propagation approaches.

2. The computational framework

As we show in this article, there are good reasons why nested multilevel and crossed effect models are learnt efficiently by different computational algorithms. However, it is constructive to first recognize what the two model classes have in common. To this effect we establish some common notation. Let $\boldsymbol{\theta}$ denote all the regression coefficients and all the factor levels, and $\boldsymbol{\gamma}$ all the unknown covariance matrices/precision matrices/precision parameters. Then, in both models the prior $\mathcal{L}(\boldsymbol{\theta} \mid \boldsymbol{\gamma})$ is a high-dimensional Gaussian with sparse dependence structure. The conditional posterior $\mathcal{L}(\boldsymbol{\theta} \mid \boldsymbol{y}, \boldsymbol{\gamma})$ is also a high-dimensional distribution with typically sparse dependence structure, and is Gaussian when the likelihood is. In crossed effect models such posterior has a tractable precision matrix with known position for zeros and known values (as functions of unknown parameters) for the non-zero elements. In Gaussian nested multilevel models the posterior might not have an invertible covariance, hence the posterior precision might not be well-defined, but when it is, it enjoys the same tractability as for crossed effect models. A fundamental difference between the two paradigms is that whereas in nested multilevel models posterior dependence structure is driven by the prior, in nested it is driven by the likelihood.

All algorithms we study in this work are based on a Gibbs sampling approach to sample $\mathcal{L}(\boldsymbol{\theta}, \boldsymbol{\gamma} \mid \boldsymbol{y})$, whereby they iterate sampling $\mathcal{L}(\boldsymbol{\theta} \mid \boldsymbol{y}, \boldsymbol{\gamma})$ and $\mathcal{L}(\boldsymbol{\gamma} \mid \boldsymbol{y}, \boldsymbol{\theta})$. Nevertheless, in our numerical studies we compare against different strategies, in particular Hamiltonian Monte Carlo (HMC) and mean field Variational Bayes as delivered by the computational engine STAN, and we discuss other alternatives, such as INLA, when is due.

Sampling $\mathcal{L}(\boldsymbol{\gamma} \mid \boldsymbol{y}, \boldsymbol{\theta})$ is easy, it involves a few gamma and low-dimensional Wishart simulations and is pretty much the same for the two model classes. On the other hand, $\mathcal{L}(\boldsymbol{\theta} \mid \boldsymbol{y}, \boldsymbol{\gamma})$ is high-dimensional, sampling it efficiently is non-trivial and it is in this respect that our methods differ. The main three paradigms we develop are Gibbs sampling (Section 3), methods based on sparse linear algebra techniques (Section 4) and belief propagation (Section 5). It is important to realize that the case of Gaussian $\mathcal{L}(\boldsymbol{\theta} \mid \boldsymbol{y}, \boldsymbol{\gamma})$ is not particularly easier in high-dimensions, even though direct methods based on the Cholesky decomposition exist. In fact, in the article we prove that in certain crossed effect models the complexity of the Gibbs sampler we propose for $\mathcal{L}(\boldsymbol{\theta} \mid \boldsymbol{y}, \boldsymbol{\gamma})$ is better than that of direct methods based on sparse linear algebra. We also obtain various other results about the lack of scalability of sparse linear algebra methods for such models.

Our methodological contributions and theoretical results on scalability refer to sampling $\mathcal{L}(\boldsymbol{\theta} \mid \boldsymbol{y}, \boldsymbol{\gamma})$. The details of sampling $\mathcal{L}(\boldsymbol{\gamma} \mid \boldsymbol{y}, \boldsymbol{\theta})$ (as well as certain related acceleration tricks, e.g., parameter expansion) are given in Section 6 together with our large scale numerical illustrations. Obtaining rigorous results for the scalability of the joint algorithm that samples both $\boldsymbol{\theta}$ and $\boldsymbol{\gamma}$ is very hard, beyond the scope of this work (see Section 7.2 for more details) and unlikely to lead to different conclusions than those we obtain in our analysis. Detailed numerical studies give promise that the intuitions from sampling $\mathcal{L}(\boldsymbol{\theta} \mid \boldsymbol{y}, \boldsymbol{\gamma})$ carry over to sampling $\mathcal{L}(\boldsymbol{\theta}, \boldsymbol{\gamma} \mid \boldsymbol{y})$.

2.1. A note on the notation

For the rest of the article it is helpful to establish a complexity nomenclature. We write $C = \mathcal{O}(N)$ to mean that there are constants, c_1, c_2 such that $c_1 < C/N < c_2$. In the article we will be interested how complexity varies as a function of N and p, hence "constants" will refer to quantities that do not vary as N and p do. Our theoretical calculations involve non-asymptotic computations, the proofs of our results provide explicit formulae for the constants involved.

3. Crossed effect models and Gibbs sampling

3.1. Methodology

We first discuss the case with no fixed regressor $\boldsymbol{\beta}$, for notational simplicity, and return to the general case at the end of this subsection. The proposed sampler is based on partitioning the $p = (1 + I_1 + \cdots + I_K) \times L$ unknown parameters into $K+1$ blocks, $\boldsymbol{\theta} = (\boldsymbol{a}^{(0)}, \boldsymbol{a}^{(1)}, \ldots, \boldsymbol{a}^{(K)})$, and performing the following sequence of block updates:

$$(\boldsymbol{a}^{(0)}, \boldsymbol{a}^{(k)}) \sim \mathcal{L}(\boldsymbol{a}^{(0)}, \boldsymbol{a}^{(k)} \mid \boldsymbol{y}, \boldsymbol{\gamma}, \boldsymbol{a}^{(-0,-k)}) \qquad k = 1, \ldots, K\,, \tag{6}$$

where $\boldsymbol{a} = (\boldsymbol{a}^{(k)})_{k=0}^{K}$ and $\boldsymbol{a}^{(-0,-k)} = (\boldsymbol{a}^{(j)})_{j \notin \{0,k\}}$. In terms of the induced Markov chain, the updates in (6) are equivalent to "collapsing" the global parameters $\boldsymbol{a}^{(0)}$ and updating $\boldsymbol{a}^{(k)} \sim \mathcal{L}(\boldsymbol{a}^{(k)} \mid \boldsymbol{y}, \boldsymbol{\gamma}, \boldsymbol{a}^{(-0,-k)})$, which explains the characterisation "collapsed". For Gaussian likelihoods, exact simulation from (6) can be performed efficiently by first sampling $\boldsymbol{a}^{(0)} \sim \mathcal{L}(\boldsymbol{a}^{(0)} \mid \boldsymbol{y}, \boldsymbol{\gamma}, \boldsymbol{a}^{(-0,-k)})$ and then sampling $\boldsymbol{a}^{(k)}_{i_k} \sim \mathcal{L}(\boldsymbol{a}^{(k)}_{i_k} \mid \boldsymbol{y}, \boldsymbol{\gamma}, \boldsymbol{a}^{(-k)})$ independently over i_k; see the Appendix for closed form expressions for these conditional distributions.

For general likelihoods, we propose a Markov chain update invariant with respect to $\mathcal{L}(\boldsymbol{a}^{(0)}, \boldsymbol{a}^{(k)} \mid \boldsymbol{y}, \boldsymbol{\gamma}, \boldsymbol{a}^{(-0,-k)})$. One could apply a default gradient-based sampler directly but we do not expect this to work well. The target is high-dimensional there is strong posterior dependence between $\boldsymbol{a}^{(0)}$ and $\boldsymbol{a}^{(k)}$. The prior precision does not capture this dependence in crossed effect models, as discussed in Section 2, thus ruling out efficient gradient-based samplers that precondition using the prior precision, as for example in Titsias and Papaspiliopoulos (2018).

Instead, we propose to explicitly leverage the sparse conditional independence structure of $\mathcal{L}(\boldsymbol{a}^{(0)}, \boldsymbol{a}^{(k)} \mid \boldsymbol{y}, \boldsymbol{\gamma}, \boldsymbol{a}^{(-0,-k)})$. We use local hierarchical centering within each block $(\boldsymbol{a}^{(0)}, \boldsymbol{a}^{(k)})$, which consists of introducing centered parameters $\boldsymbol{\xi}^{(k)} = (\boldsymbol{\xi}^{(k)}_{i_k})_{i_k=1,\ldots,I_k}$ defined as $\boldsymbol{\xi}^{(k)}_{i_k} = \boldsymbol{a}^{(0)} + \boldsymbol{a}^{(k)}_{i_k}$, and then replacing the k-th update in (6) with:

$$\boldsymbol{a}^{(0)} \sim \mathcal{L}(\boldsymbol{a}^{(0)} \mid \boldsymbol{y}, \boldsymbol{\gamma}, \boldsymbol{a}^{(-0,-k)}, \boldsymbol{\xi}^{(k)}) = \mathcal{L}(\boldsymbol{a}^{(0)} \mid \boldsymbol{\xi}^{(k)}) \tag{7}$$

$$\boldsymbol{\xi}^{(k)}_{i_k} \sim \mathcal{L}(\boldsymbol{\xi}^{(k)}_{i_k} \mid \boldsymbol{y}, \boldsymbol{\gamma}, \boldsymbol{a}^{(-k)}) \qquad i_k = 1, \ldots, I_k\,. \tag{8}$$

The above strategy is robust to high-dimensionality by explicitly exploiting conditional independence across in (8), which leads to I_k independent L-dimensional updates. Additionally, it avoids mixing issues arising from the strong dependence between $\boldsymbol{a}^{(0)}$ and $\boldsymbol{a}^{(k)}$ by relying instead on the weaker posterior dependence between $\boldsymbol{a}^{(0)}$ and the centred parameters $\boldsymbol{\xi}^{(k)}$. After performing the updates in (7)-(8) for a given k, one computes $\boldsymbol{a}^{(k)}_{i_k} = \boldsymbol{\xi}^{(k)}_{i_k} - \boldsymbol{a}^{(0)}$ for $i_k = 1, \dots, I_k$ in order to recover the original parametrization $\boldsymbol{a}^{(k)}$ and proceed. Direct sampling from (7) is straightforward, since

$$\mathcal{L}(\boldsymbol{a}^{(0)} \mid \boldsymbol{\xi}^{(k)}) = \mathcal{N}\left((\boldsymbol{T}_{pr} + I_k \boldsymbol{T}_k)^{-1} \Big(\boldsymbol{T}_{pr} \boldsymbol{\mu}_{pr} + \boldsymbol{T}_k \sum_{i_k=1}^{I_k} \boldsymbol{\xi}^{(k)}_{i_k} \Big), (\boldsymbol{T}_{pr} + I_k \boldsymbol{T}_k)^{-1} \right).$$

The full conditionals in (8) are not available in closed form in general, thus we perform a Metropolis-Hastings update that leaves them invariant. When $L = 1$ we use a second-order Metropolis-Hastings proposal defined in the Appendix with no tuning parameters and cheap to implement. When $L > 1$ we use the gradient-based Metropolis-Hastings sampler of Titsias and Papaspiliopoulos (2018), which proposes new value for each $\boldsymbol{\xi}^{(k)}_i$, according to a $\mathcal{N}(\boldsymbol{m}^{(k)}_i, \boldsymbol{D}^{(k)}_i)$, with

$$\begin{aligned} \boldsymbol{m}^{(k)}_i &= \boldsymbol{C}^{(k)}_i \left(\boldsymbol{\xi}^{(k)}_i / \delta^{(k)}_i + \nabla f^{(k)}_i (\boldsymbol{\xi}^{(k)}_i - \boldsymbol{a}^{(0)}) + \boldsymbol{T}_k \boldsymbol{a}^{(0)} \right) \\ \boldsymbol{D}^{(k)}_i &= \boldsymbol{C}^{(k)}_i + \left(\boldsymbol{C}^{(k)}_i \right)^2 / \delta^{(k)}_i, \quad \boldsymbol{C}^{(k)}_i = \left(\boldsymbol{T}_k + \boldsymbol{I} / \delta^{(k)}_i \right)^{-1}, \end{aligned}$$

and $f^{(k)}_i(\boldsymbol{a}^{(k)}_i)$ the log-likelihood of $\boldsymbol{y}$ as a function of $\boldsymbol{a}^{(k)}_i$ holding other parameters fixed. The resultant acceptance probability is in the Appendix. The scalars $\delta^{(k)}_i$ are level-specific step size parameters that we tune adaptively according to the Robbins-Monro procedure described in, e.g., Algorithm 4 of Andrieu and Thoms (2008), with target acceptance rate equal to a half and learning rate at iteration t set to $t^{-0.5}$. Section 6 details the above methodology and implementation details for the case of multinomial-logit likelihood and applies it to the motivating application discussed in Section 1.2.

The above collapsed Gibbs sampling methodology provides an effective way to update the high-dimensional block of unknown parameters $\boldsymbol{a}$ and can be trivially extended to the context where the model includes also fixed regressors as in (1). The simplest strategy would be to update the global coefficients $\boldsymbol{\beta}$ from their full conditional distribution in a Gibbs or Metropolis-within-Gibbs style after the update of $\boldsymbol{a}$ detailed above. Regardless of the specific implementation, the key aspect here is that the dimensionality of $\boldsymbol{\beta}$ is much lower than the dimensionality of $\boldsymbol{a}$ in our applications of interest. More robust strategies are possible, such as updating $\boldsymbol{\beta}$ jointly with the intercept $\boldsymbol{a}^{(0)}$, but we defer the discussion of such strategies, as well as of the discussion of the case of high-dimensional $\boldsymbol{\beta}$, to future work.

3.2. Complexity

The computational complexity of the Gibbs sampler depends both on the cost per iteration and on the number of iterations required to obtain each effective sample. Recall that throughout our theoretical analysis applies to the algorithm for sampling $\mathcal{L}(\boldsymbol{\theta} \mid \boldsymbol{y}, \gamma)$, even though all our numerics are about sampling $\mathcal{L}(\boldsymbol{\theta}, \boldsymbol{\gamma} \mid \boldsymbol{y})$.

Definition 1. *The computational complexity of the Gibbs sampler is*

$$\textit{Cost}(\textit{Gibbs}) = \textit{(cost per iteration)} \times \textit{(relaxation time)}\,, \tag{9}$$

where the relaxation time refers to the reciprocal of 1 minus the rate of convergence (Rosenthal, 2003, Proposition 1).

The cost per iteration of the collapsed Gibbs sampler proposed above is of order $\mathcal{O}(KNL + KL^3 + pL^2)$, as we show now. The evaluation of the gradients terms in (3.1) has a $\mathcal{O}(NL)$ cost for each factor, since

$$\nabla f_i^{(k)}(\boldsymbol{a}_i^{(k)}) = \sum_{j\,:\,i_k[j]=i} \nabla_{\boldsymbol{a}_i^{(k)}} \log p(\boldsymbol{y}_j \mid \boldsymbol{a}) \qquad\qquad i = 1, \dots, I_k\,,$$

implies that exactly N terms of the form $\nabla_{\boldsymbol{a}_i^{(k)}} \log p(\boldsymbol{y}_j \mid \boldsymbol{a})$ for $j = 1, \dots, N$ need to be computed, at $\mathcal{O}(L)$ cost each. By similar arguments also the likelihood evaluations required by the acceptance probability computation require $\mathcal{O}(NL)$ operations per factor. Given the gradient and likelihood computations, one can eigendecompose $\boldsymbol{T}_k$ at $\mathcal{O}(L^3)$ cost and then perform the updates of $\boldsymbol{\xi}_i^{(k)}$ for all i at $\mathcal{O}(I_k L^2)$ cost. Summing over factors we obtain the $\mathcal{O}(KNL + KL^3 + pL^2)$ cost. The update from $\mathcal{L}(\boldsymbol{a}^{(0)} \mid \boldsymbol{\xi}^{(k)})$ requires $\mathcal{O}(L^3)$ operations, which does not influence the overall cost and can further be reduced to $\mathcal{O}(L^2)$ if the prior precision $\boldsymbol{T}_{pr}$ is diagonal and $\boldsymbol{T}_k$ has already been eigendecomposed.

While the relaxation time of MCMC algorithms is hard to characterize in general, that of the collapsed Gibbs sampler for Gaussian likelihood has become to a good extent understood due to the recent work in Papaspiliopoulos et al. (2020). We now provide a complexity result that builds upon Papaspiliopoulos et al. (2020, Theorem 4), the proof of which is found in the Appendix.

Definition 2. *We denote occurrence and co-occurrence counts associated to levels of different factors, as*

$$n_{ij}^{(k,\ell)} = \sum_{n=1}^{N} \mathbb{1}(i_k[n] = i, i_\ell[n] = j),$$
$$n_i^{(k)} = \sum_{n=1}^{N} \mathbb{1}(i_k[j] = i).$$

We say that a design has balanced levels $n_i^{(k)} = N/I_k$ for each factor k and level i. We define

$$\bar{n} = KN/p$$

for $p = \sum_k I_k$, to be interpreted as the average number of observed data points per factor level.

Theorem 1. *We assume balanced levels, $K = 2$, $L = 1$, and Gaussian likelihood. Let T_{aux} be the relaxation time of an auxiliary two-component deterministic-scan Gibbs sampler targeting a discrete distribution with state space $\{1, \dots, I_1\} \times \{1, \dots, I_2\}$ and probability mass function proportional to $n_{ij}^{(1,2)}$. Then, the complexity of the collapsed Gibbs sampler that samples (6) exactly is*

$$Cost(Gibbs) = \mathcal{O}((2N + p)\min\{\bar{n}, T_{aux}\}),$$

where the constant depends only on $\boldsymbol{\gamma}$ and not on N, p.

The factor $2N + p$ comes from the cost per iteration, and $\min\{\bar{n}, T_{aux}\}$ comes from the relaxation time. In Section 7 we discuss the dependence of the cost on $\boldsymbol{\gamma}$, and its implications for theory and modelling. To get some intuition on the implications of this result, it is convenient to recall the interpretation of the model as a recommender system when $K = 2$, as discussed in Section 1.2. Note that $\bar{n}$ can be interpreted as the average number of products rated by a customer; it is precisely this number when $I_1 = I_2$ and the design has balanced levels. In sparse designs, increasing values of N will not be associated with increasing values of $\bar{n}$ (more products and customers, but each customer rates a bounded number of products). In such regimes the sampler is scalable. In less sparse designs where $\bar{n}$ increases with N, the contingency table is more populated, and provided it is populated enough for the auxiliary Markov chain to mix well, the sampler will again be scalable. This intuition is numerically supported in the simulations in Papaspiliopoulos et al. (2020), and can be seen in those of Figure 4 later in this article. We return in Section 4.4 with more results along this direction (making comparisons to sparse linear algebra methods) and in Section 7 for pointers to theory about the mixing of this auxiliary Markov chain.

Theorem 1 holds for Gaussian likelihoods, but we see this more an artifact of our strategy in proving the result, as opposed to the nature of the result itself, which we believe relates to the conditional independence structure in the model. We have corroborated the validity of this finding in a number of simulation studies, one of which we include here. We consider a completely missing at random design, where each cell in the contingency table is observed with probability 0.1 and is blank otherwise. For the non-empty cells we simulate observations either from a Gaussian distribution, $\mathcal{L}(y_j \mid \eta_j) = \mathcal{N}(\eta_j, 1)$ or a binomial one, $\mathcal{L}(y_j \mid \eta_j) = Binomial(1, (1 + \exp(-\eta_j)^{-1})$, and we use the corresponding likelihood when we learn the model. We consider datasets simulated from the correctly specified model, for $L = 1$, $K = 2$, $I_1 = I_2$ and increasing values of I_1, which means that p, N and $\bar{n}$ grow with I_1 (see Section 4.4 for mode detailed related calculations). We generate all elements of $\boldsymbol{\theta}$ from a standard Gaussian distribution and data points from the respective likelihoods.

We test the performance of the collapsed second-order Metropolis-within-Gibbs sampler (see Appendix for details, it is the scheme that we prefer for $L = 1$ and involves no tuning parameters). To put in perspective the benefit of collapsing, we also compare performance to that of a vanilla (non-collapsed) sampler that updates the components of $\boldsymbol{\theta}$ sequentially. We treat the precision parameters, τ_k, as unknown and assign them a unit information $Gamma(1/2, 1/2)$. Since the exact relaxation time is not analytically available for the algorithms we implement, we monitor the empirical estimates of *integrated autocorrelation times* for various parameters; see the Appendix for the definition of this quantity and how it is computed empirically; if this quantity remains constant with respect to N it suggests that the corresponding parameter has relaxation time $\mathcal{O}(N)$. In our study, we report results averaged over 10 datasets, for each of the simulation settings. Figure 3 reports the estimates for $a^{(0)}$, $I_k^{-1}\sum_{i=1}^{I_k} a_i^{(k)}$, and for τ_k^{-1}, for $k = 1, 2$. Note that whereas the simulation of data was done with different values of I_1, here we show the results as a function of the implied N. The results suggest that the two

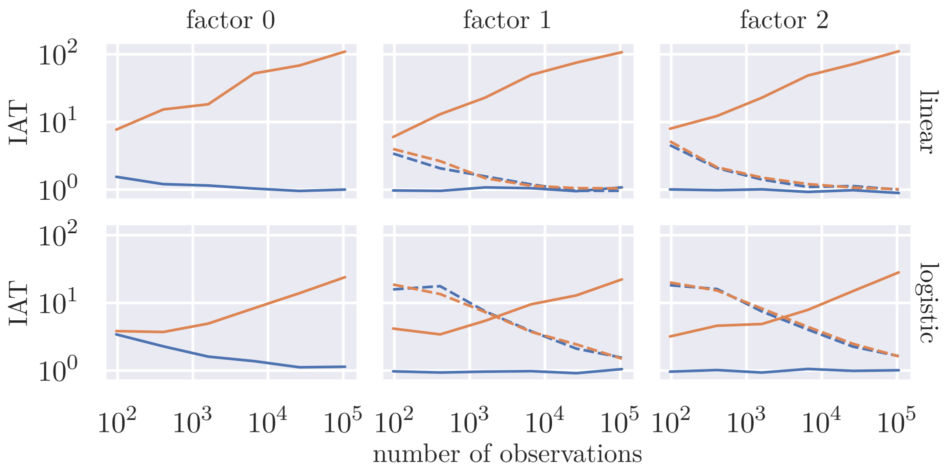

Figure 3.: Integrated autocorrelation time estimates as a function of N for the collapsed (blue) and the vanilla (orange) Metropolis-within-Gibbs sampler. Solid lines refer to $a^{(0)}$ and $I_k^{-1}\sum_{i_k=1}^{I_k} a_{i_k}^{(k)}$, and dashed to τ_k^{-1}, for $k = 1, 2$.

likelihoods lead to highly comparable behaviors in terms of sampling efficiency. There is a slight increase in integrated autocorrelation times for the unknown variances when moving from Gaussian to binomial data, which may be due to posterior skewness, but the increase is minor, roughly a factor of 2. More crucially, the results for the collapsed Metropolis-within-Gibbs sampler are indicative of a relaxation time uniformly bounded in N. Note that here $\bar{n}$ diverges as $N \to \infty$, which suggests that it is T_{aux} which comes to rescue. We return in Section 7 with some pointers for future directions on the behaviour of T_{aux} on random observational designs. Overall, the results support the claim that both the transition from Gibbs to Metropolis-within-Gibbs, from known to unknown γ and from Gaussian to non-Gaussian likelihood do not have a major impact on the resulting MCMC mixing behaviour.

3.3. Related literature and alternative approaches

Early work on Bayesian computation for crossed effect models includes Vines et al. (1996) and Gelfand et al. (1996, Section 6), who discuss, respectively, the use of identifiability constraints and reparametrizations for computational purposes. Gao and Owen (2017,

2020) provide a systematic discussion of the super-linear cost of standard frequentist and Bayesian fitting procedures, including an argument for $\mathcal{O}(N^{3/2})$ complexity of the vanilla Gibbs sampler in some specific setting, and develop a scalable method of moments for 2-factor crossed effect models. Papaspiliopoulos et al. (2020) provide a detailed analysis of the Gibbs sampler complexity, covering also sparse balanced designs and $K \geq 2$ factors, and propose a scalable collapsed Gibbs sampler for Gaussian likelihood; the method we develop in 3.1 is the extension of their paradigm to non-Gaussian likelihoods. Ghosh et al. (2020) propose a coordinate-wise descent method for computing the MAP estimator (phrased in their article as a backfitting procedure to compute generalized least squares estimates) that has close connections to collapsed Gibbs sampling. They prove $\mathcal{O}(N)$ complexity results also for designs with some degree of unbalancedness, their arguments are based on simple but effective concentration inequalities and linear algebra techniques.

Zanella and Roberts (2020, Theorem 5) show that for crossed effect models with $K = 2$ factors, global reparametrizations are not sufficient to recover $\mathcal{O}(N)$ complexity. This result provides motivation for the local reparametrization methodology implemented in (6)-(8). A further motivation for local hierarchical centering comes from Papaspiliopoulos et al. (2007); the sizes of the variance of the different terms is such that makes conditional posterior dependence weaker between the centered $(\boldsymbol{a}^{(0)}, \boldsymbol{\xi}^{(k)})$ than the non-centered $(\boldsymbol{a}^{(0)}, \boldsymbol{a}^{(k)})$ pair.

A common practice among practitioners is the imposition of identifiability constraints within each factor. Of course, such constraints are not needed for the inference to make sense in a Bayesian formulation, if needed they can be imposed a posteriori and different constraints will lead to different inferences. Nevertheless, from the point of view of this article it is worth considering their impact on algorithmic performance. Theorem 6 of Zanella and Roberts (2020) derives the relaxation times of the vanilla Gibbs sampler for crossed effect models with Gaussian likelihood. Some constraints can make the vanilla Gibbs sampler scalable, whereas others cannot. Unfortunately, those that do, lead to difficult sampling problems when considering non-Gaussian likelihoods.

One could combine collapsing with techniques that seek to reduce posterior dependence between $\boldsymbol{\theta}$ and $\boldsymbol{\gamma}$, such as parameter expansion (Liu and Wu, 1999; Meng and Van Dyk, 1999). However, while useful and applicable, in the simulation studies of Papaspiliopoulos et al. (2020) for crossed effect models with Gaussian likelihoods, this strategy was found to have little impact on the resulting MCMC efficiency and it did not appear to change the overall complexity of the parent algorithm.

Menictas et al. (2019) and Goplerud (2020) propose mean field variational Bayes procedures for crossed models with Gaussian and logistic likelihoods, respectively, motivated by the overly high computational cost of Laplace approximations and HMC sampling for such models. See also Vallejos et al. (2015) for applications of crossed effect models to the analysis of single-cell sequencing data.

Many popular software for models with Gaussian latent variables, such as *lme4* (Bates et al., 2015) or *INLA* (Rue et al., 2009), perform approximate integration of $\boldsymbol{\theta}$ using variants of the Laplace approximation. These approaches rely on sparse linear algebra techniques. The next section studies such techniques in detail and compares their cost to Gibbs sampling, also in the context of crossed effect models. Hence, we discuss the merits of such approaches for crossed effect models in the next section.

4. Sparse linear algebra and scalable computation

Throughout this section we assume Gaussian likelihood and an invertible prior covariance, in which case the posterior precision associated to the Gaussian posterior $\mathcal{L}(\boldsymbol{\theta} \mid \boldsymbol{y}, \gamma)$ is well defined and will be denoted by $\boldsymbol{Q}$. These assumptions rule out certain classes of nested multilevel models for which the covariance matrix is semi-definite. The ideas we develop here are useful beyond Gaussian likelihoods, and this is explored in Section 7. Chapter 2 of Rue and Held (2005) is an excellent reference for background on the type of arguments we use in the following subsections.

4.1. Sampling Gaussian posteriors as a linear algebra problem

When $\mathcal{L}(\boldsymbol{\theta} \mid \gamma) = \mathcal{N}(\boldsymbol{m}, \boldsymbol{V}^{-1})$, and $-2\log p(\boldsymbol{y} \mid \boldsymbol{\theta}, \gamma) = \boldsymbol{\theta}^T \boldsymbol{U}\boldsymbol{\theta} - 2\boldsymbol{y}^T\boldsymbol{R}^T\boldsymbol{\theta}$ (up to constants in $\boldsymbol{\theta}$), then $\mathcal{L}(\boldsymbol{\theta} \mid \boldsymbol{y}, \gamma)$ is also Gaussian, with precision $\boldsymbol{Q} = \boldsymbol{U} + \boldsymbol{V}$. By exploiting the graphical model structure and its sparsity one can often easily work out the elements in $\boldsymbol{Q}$, see for example the expressions for nested multilevel and crossed effect models in (18) and (19), respectively. Additionally, let $\boldsymbol{L}$ be the lower-triangular Cholesky factor of $\boldsymbol{Q}$; when and how this can be computed efficiently is discussed in Section 4.2. Then, a sample from the posterior $\mathcal{L}(\boldsymbol{\theta} \mid \boldsymbol{y}, \gamma)$ is obtained by solving the following two systems, where $\boldsymbol{z}$ is a standard Gaussian vector:

$$\begin{aligned} \boldsymbol{L}\boldsymbol{w} &= \boldsymbol{R}\boldsymbol{y} + \boldsymbol{V}\boldsymbol{m} \\ \boldsymbol{L}^T\boldsymbol{\theta} &= \boldsymbol{w} + \boldsymbol{z}. \end{aligned} \tag{10}$$

As we see in Section 4.2 below, $\boldsymbol{L}$ can be computed columnwise from first to last column. Hence, the computation of $\boldsymbol{L}$ and the simultaneous solution of the top equation in (10) by forward substitution, can thought of as a *forward pass*. Having completed the forward pass, we can then solve the second equation in (10) by backward substitution, in what we can think of as a *backward pass*. The computation of $\boldsymbol{L}$ is the dominant cost in this approach, which motivates the following definition.

Definition 3. *The computational complexity of sampling from $\mathcal{L}(\boldsymbol{\theta} \mid \boldsymbol{y}, \gamma)$ by obtaining $\boldsymbol{L}$ and solving (10) will be denoted $Cost(SLA)$, and it is defined as the number of "flops" required to compute the Cholesky factor $\boldsymbol{L}$ according to the recursive equations in (15) given in the sequel.*

The remainder of this section delves into the cost of the Cholesky computations, first reviewing general facts and then discussing their implications for nested multilevel and crossed effect models.

4.2. The Cholesky factor

Here is a probabilistic perspective on the Cholesky factor and an algorithm to compute its elements column-wise; the resultant algorithm can also be obtained using linear algebra arguments (see e.g. Golub and van Loan (2013, Section 4.2.5) or Rue and Held, 2005, Section 2.4.1). Suppose that $\mathcal{L}(\boldsymbol{\theta}) = \mathcal{N}(\mathbf{0}, \boldsymbol{Q}^{-1})$, with $\boldsymbol{Q} = \boldsymbol{L}\boldsymbol{L}^T$, where $\boldsymbol{L}$ is the lower-triangular Cholesky factor, and we think $\boldsymbol{\theta}$ organized in M blocks, $\boldsymbol{\theta} = (\boldsymbol{\theta}_1, \dots, \boldsymbol{\theta}_M)^T$, with the matrices organized accordingly. Then, a sample of $\boldsymbol{\theta}$ can be obtained by solving the linear system $\boldsymbol{L}^T\boldsymbol{\theta} = \boldsymbol{z}$, for $\boldsymbol{z} \sim \mathcal{N}(\mathbf{0}, \boldsymbol{I})$, by backwards substitution. Effectively, what we obtain this way is a backwards decomposition of the joint law of $\boldsymbol{\theta}$:

$$\mathcal{L}(\boldsymbol{\theta}) = \mathcal{L}(\boldsymbol{\theta}_M) \otimes \mathcal{L}(\boldsymbol{\theta}_{M-1} \mid \boldsymbol{\theta}_M) \otimes \cdots \otimes \mathcal{L}(\boldsymbol{\theta}_1 \mid \boldsymbol{\theta}_2, \dots, \boldsymbol{\theta}_M), \tag{11}$$

where $\otimes$ above denotes convolution of the probability distributions. The triangular linear system above, implies then that

$$\begin{aligned} \mathcal{L}(\boldsymbol{\theta}_m \mid \boldsymbol{\theta}_{m+1}, \dots, \boldsymbol{\theta}_M) &= \mathcal{N}\left(-\boldsymbol{L}_{mm}^{-1} \sum_{\ell > m} \boldsymbol{L}_{\ell m}\boldsymbol{\theta}_\ell, \boldsymbol{L}_{mm}^{-1}\boldsymbol{L}_{mm}^{-T}\right), \quad m < M, \\ \mathcal{L}(\boldsymbol{\theta}_M) &= \mathcal{N}\left(\mathbf{0}, \boldsymbol{L}_{MM}^{-1}\boldsymbol{L}_{MM}^{-T}\right), \end{aligned} \tag{12}$$

thus the m-th column of $\boldsymbol{L}$ characterizes the distribution of $\boldsymbol{\theta}_m$ conditionally on $\boldsymbol{\theta}_{m+1}, \dots, \boldsymbol{\theta}_M$ but marginally with respect to $\boldsymbol{\theta}_1, \dots, \boldsymbol{\theta}_{m-1}$. It is well-known that the full conditional distributions are

$$\mathcal{L}(\boldsymbol{\theta}_m \mid \boldsymbol{\theta}_{-m}) = \mathcal{N}\left(-\boldsymbol{Q}_{mm}^{-1} \sum_{\ell > m} \boldsymbol{Q}_{\ell m}\boldsymbol{\theta}_\ell, \boldsymbol{Q}_{mm}^{-1}\right). \tag{13}$$

The above observations, together with a re-arrangement of the basic identity:

$$\begin{aligned} p(\boldsymbol{\theta}_m \mid \boldsymbol{\theta}_{-m}) &\propto \prod_{\ell \le m} p(\boldsymbol{\theta}_\ell \mid \boldsymbol{\theta}_{\ell+1}, \dots, \boldsymbol{\theta}_M), \quad m < M \\ p(\boldsymbol{\theta}_M \mid \boldsymbol{\theta}_{-M}) &\propto p(\boldsymbol{\theta}_M) \prod_{\ell < M} p(\boldsymbol{\theta}_\ell \mid \boldsymbol{\theta}_{\ell+1}, \dots, \boldsymbol{\theta}_M) \end{aligned} \tag{14}$$

obtain the column-wise recursion for the elements of the Cholesky factor:

$$\begin{aligned} \boldsymbol{L}_{mm}\boldsymbol{L}_{mm}^T &= \boldsymbol{Q}_{mm} - \sum_{\ell=1}^{m-1} \boldsymbol{L}_{m\ell}\boldsymbol{L}_{m\ell}^T \\ \boldsymbol{L}_{mm}\boldsymbol{L}_{jm} &= \boldsymbol{Q}_{jm} - \sum_{\ell=1}^{m-1} \boldsymbol{L}_{m\ell}\boldsymbol{L}_{j\ell}, \quad j > m. \end{aligned} \tag{15}$$

It is well known, and can be seen directly from (13), that $\boldsymbol{\theta}_m$ and $\boldsymbol{\theta}_j$ are conditionally independent given the rest of the variables if and only if $\boldsymbol{Q}_{jm} = \mathbf{0}\mathbf{0}^T$. Hence sparsity in the precision matrix corresponds to missing edges in the conditional independence graph, which we denote as $G_{\boldsymbol{Q}}$. Also known and obvious from (12) above, is that for $m < j$, $\boldsymbol{L}_{jm} = \mathbf{0}\mathbf{0}^T$ if and only if $\boldsymbol{\theta}_m$ and $\boldsymbol{\theta}_j$ are independent given the *future set* of $\boldsymbol{\theta}_m$ excluding $\boldsymbol{\theta}_j$, i.e., $\boldsymbol{\theta}_m \perp \boldsymbol{\theta}_j | \boldsymbol{\theta}_{\{(m+1):M\}\setminus j}$ (Rue and Held, 2005, Theorem 2.8). Therefore, even when $\boldsymbol{Q}$ is sparse, as in nested and crossed effect models, $\boldsymbol{L}$ might not be and the order we assign to variables when we define the vector to be sampled matters enormously.

The number of non-zero elements in $\boldsymbol{L}$ can be predicted from $G_{\boldsymbol{Q}}$. Indeed, a sufficient condition to ensure $\boldsymbol{L}_{jm} = \mathbf{0}\mathbf{0}^T$ for $m < j$ is that the future set of $\boldsymbol{\theta}_m$ separates it from $\boldsymbol{\theta}_j$ in $G_{\boldsymbol{Q}}$. This motivates defining the number of possible non-zero blocks in $\boldsymbol{L}$ as $n_{\boldsymbol{L}} = \sum_{m=1}^{M} n_{\boldsymbol{L},m}$ where

$$n_{\boldsymbol{L},m} = \left|\{j \geq m \,:\, \text{the future set of } \boldsymbol{\theta}_m \text{ does not separate it from } \boldsymbol{\theta}_j \text{ in } G_{\boldsymbol{Q}}\}\right|. \tag{16}$$

Thus, the Cholesky factor $\boldsymbol{L}$ involves $n_{\boldsymbol{L}} - n_{\boldsymbol{Q}} \geq 0$ additional potential non-zero blocks compared to the original matrix $\boldsymbol{Q}$; here $n_{\boldsymbol{Q}}$ denotes the number of non-zero blocks in the lower triangular part of $\boldsymbol{Q}$. Such additional non-zeros terms are commonly referred as *fill-ins*. The actual number or non-zero blocks in $\boldsymbol{L}$ may be lower than $n_{\boldsymbol{L}}$, see the Appendix for an example. This, however, cannot be predicted by the structure of $G_{\boldsymbol{Q}}$ alone and relies on numerical cancellations in the recursive equations in (15). Also, for each given $G_{\boldsymbol{Q}}$ there is always a $\boldsymbol{Q}$ such that all $n_{\boldsymbol{L}}$ values are non-zero (e.g. Gilbert, 1994, Theorem 4.1). Since $n_{\boldsymbol{L}}$ depends on the ordering of the variables in $\boldsymbol{\theta}$, standard algorithms for Cholesky factorizations of sparse matrices proceed in two steps: first they try to find an ordering of variables that reduces $n_{\boldsymbol{L}}$ as much as possible, and then compute the corresponding Cholesky factor using (15). Finding the ordering that minimizes $n_{\boldsymbol{L}}$ is NP-hard, but various heuristic strategies to find good orderings are available (see e.g. Section 11.1 of Golub and van Loan, 2013 for a review) and are implemented in standard sparse linear algebra software. The effectiveness of the resulting ordering is often measured in terms of the *fill-in ratio* defined as $n_{\boldsymbol{L}}/n_{\boldsymbol{Q}}$, and values closer to 1 are desirable as they indicate that the sparsity of $\boldsymbol{L}$ is closer to that of $\boldsymbol{Q}$.

Sparsity in $\boldsymbol{L}$ has direct consequences on the computational cost required to compute it - although it has to be appreciated that a sparse Cholesky is not necessarily computable efficiently! The following theorem quantifies this connection; the result does not show dependence of the cost on the size of each block in the partitioning, since this is not a priority in our applications; we are interested instead in the large M case.

Theorem 2.

$$\mathcal{O}\left(n_{\boldsymbol{L}}^2/M\right) \leq Cost(SLA) = \mathcal{O}\left(\sum_{m=1}^{M} n_{\boldsymbol{L},m}^2\right) \leq \mathcal{O}\left(n_{\boldsymbol{L}}^{1.5}\right). \tag{17}$$

The equality and lower bound in (17) are well-known, but the upper bound is more involved, and we have not been able to find it in the literature. The Appendix contains the proof of Theorem 2. Note that trivially the result also implies

$$Cost(SLA) \geq \mathcal{O}(n_{\boldsymbol{Q}}^2/M).$$

When $\boldsymbol{Q}$ is a dense matrix we have $n_{\boldsymbol{L}} = \mathcal{O}\left(M^2\right)$ and thus the lower and upper bounds in (17) coincide, being both cubic in M, and they are both tight. For sparse matrices, instead, the two bounds can differ up to a $\mathcal{O}\left(M^{0.5}\right)$ multiplicative factor and each can be tight depending on the sparsity pattern. For example, the lower bound is tight if $\boldsymbol{Q}$ is a diagonal matrix or, more generally, a banded matrix. In this case, denoting the bandwidth of $\boldsymbol{Q}$ by d, we have $n_{\boldsymbol{L}} = \mathcal{O}(Md)$ and $Cost(SLA) = \mathcal{O}(Md^2)$, which implies that the lower bound is tight while the upper bound is off by a $\mathcal{O}\left((M/d)^{0.5}\right)$ factor. On the contrary, for a matrix $\boldsymbol{Q}$ with a dense $M^{0.5} \times M^{0.5}$ sub-matrix and diagonal elsewhere we have $n_{\boldsymbol{L}} = \mathcal{O}(M)$ and $Cost(SLA) = \mathcal{O}(M^{1.5})$, meaning that the upper bound is tight while the lower bound is off by a $\mathcal{O}\left(M^{0.5}\right)$ factor.

The above discussion implies that both the degree of sparsity in $\boldsymbol{L}$ and the cost of computing it, will depend on the sparsity pattern in $\boldsymbol{Q}$. Thus, we now consider nested and crossed models separately in order to assess how effective sparse linear algebra techniques are for these class of models.

4.3. Nested multilevel models

We now specialize to nested multilevel models as in (5) with $\mathcal{L}(\boldsymbol{y}_{i_1\ldots i_k} \mid \boldsymbol{\eta}_{i_1\ldots i_k}) = \mathcal{N}(\boldsymbol{\eta}_{i_1\ldots i_k}, \tau^{-1}_{i_1\ldots i_k}\boldsymbol{I})$; recall that according to our notation the dimension of the regression coefficients $\boldsymbol{\beta}_{i_1\ldots i_k}$ is denoted by L. Since the actual ordering of the nodes in the graphical model is critical to sparse linear algebra methods and not fixed in advance, we refer to the elements of $\boldsymbol{Q}$ by indicating what blocks of regression coefficients they refer to rather than labeling the blocks with ordinal indices, e.g., we write $\boldsymbol{Q}[\boldsymbol{\beta}_{i_1\cdots i_k}, \boldsymbol{\beta}_{i_1\cdots i_{k-1}}]$ to refer to the sub-matrix of $\boldsymbol{Q}$ that corresponds to $\boldsymbol{\beta}_{i_1\cdots i_k}$ and $\boldsymbol{\beta}_{i_1\cdots i_{k-1}}$ in the nested multilevel model. For the nested multilevel models, $\boldsymbol{Q}$ consists of blocks of 0's except in the following positions (with the obvious additional non-zero blocks due to symmetry):

$$\begin{aligned}
\boldsymbol{Q}[\boldsymbol{\beta}_{i_1\cdots i_k}, \boldsymbol{\beta}_{i_1\cdots i_{k-1}}] &= -\boldsymbol{\Sigma}^{-1}_{i_1\cdots i_{k-1}} \boldsymbol{A}_{i_1\cdots i_k} \\
\boldsymbol{Q}[\boldsymbol{\beta}_{i_1\cdots i_k}, \boldsymbol{\beta}_{i_1\cdots i_k}] &= \boldsymbol{\Sigma}^{-1}_{i_1\cdots i_{k-1}} + n_{i_1\cdots i_k} \boldsymbol{A}^T_{i_1\cdots i_{k+1}} \boldsymbol{\Sigma}^{-1}_{i_1\cdots i_k} \boldsymbol{A}_{i_1\cdots i_{k+1}} \\
&\quad + \tau_{i_1\cdots i_k} \boldsymbol{X}^T_{i_1\cdots i_k} \boldsymbol{X}_{i_1\cdots i_k}, \quad 1 < k < K,
\end{aligned} \tag{18}$$

where in the second equation the second term is missing when $k = K$ and the first term is $\boldsymbol{T}_{pr}$ when $k = 1$, and throughout $n_{i_1\cdots i_k}$ is the number of offsprings of node $\boldsymbol{\beta}_{i_1\cdots i_k}$ in the graph.

In view of the future set argument laid out in Section 4.2 a good ordering of the variables in nested multilevel models is what we will call "depth-last". According to this, we place $\boldsymbol{\beta}_0$ last, then the $\boldsymbol{\beta}_i$'s (the order among them is irrelevant), then the $\boldsymbol{\beta}_{ij}$'s, and so on and so forth, until we reach the level furthest from the root. The the implied stacked vector of regression parameters $\boldsymbol{\theta}$ is organized in p/L blocks, the parent of a node (i.e., an L-dimensional regression coefficient) is always in its future set, and as a result the only non-zero elements are $\boldsymbol{L}[\boldsymbol{\beta}_{i_1\ldots i_k}, \boldsymbol{\beta}_{i_1\ldots i_k}]$ and $\boldsymbol{L}[\boldsymbol{\beta}_{i_1\ldots i_k}, \boldsymbol{\beta}_{i_1\ldots i_{k-1}}]$. Hence, $n_{\boldsymbol{Q}} = n_{\boldsymbol{L}}$, meaning that the fill-in ratio equals the optimal value of 1. Sparse linear algebra is scalable in this framework as the following proposition formalizes.

Proposition 1. *For nested multilevel models with depth-last ordering we have*

$$Cost(SLA) = \mathcal{O}(N + p)\,.$$

The result can be easily obtained from existing results in sparse linear algebra literature, hence we omit a proof. An alternative constructive proof is via the connection of sparse linear algebra with "depth-last" ordering to belief propagation, worked out in Section 5.3.

4.4. Crossed effect models

In this section we consider crossed effect models as in (1), with $\mathcal{L}(\boldsymbol{y}_j \mid \boldsymbol{\eta}_j) = \mathcal{N}(\boldsymbol{\eta}_j, \tau^{-1}\boldsymbol{I})$, and we ignore the linear regression coefficients $\boldsymbol{\beta}$ for simplicity, as they are typically much lower dimensional than the crossed categorical effects. Recall that in our generic formulation each level of each factor, say $\boldsymbol{a}_i^{(k)}$, is L-dimensional. Then, according to the notation established in Definition 2 and Section 4.3, the non-zero blocks of the precision matrix are

$$\begin{aligned} \boldsymbol{Q}[\boldsymbol{a}^{(0)}, \boldsymbol{a}^{(0)}] &= \boldsymbol{T}_{pr} + N\tau\boldsymbol{I}\,, \quad & \boldsymbol{Q}[\boldsymbol{a}^{(0)}, \boldsymbol{a}_i^{(k)}] &= n_i^{(k)}\tau\boldsymbol{I} \\ \boldsymbol{Q}[\boldsymbol{a}_i^{(k)}, \boldsymbol{a}_i^{(k)}] &= \boldsymbol{T}_k + n_i^{(k)}\tau\boldsymbol{I}\,, \quad & \boldsymbol{Q}[\boldsymbol{a}_i^{(k)}, \boldsymbol{a}_j^{(\ell)}] &= n_{ij}^{(k,\ell)}\tau\boldsymbol{I}. \end{aligned} \tag{19}$$

We concentrate on the important special case $K = 2$, $L = 1$, and we make the following structural assumption (recall from Section 4.2 that $G_{\boldsymbol{Q}}$ is the conditional independence graph associated to $\boldsymbol{Q}$).

Assumption 1. *The number of edges in $G_{\boldsymbol{Q}}$ is $\mathcal{O}(N)$.*

Assumption 1 focuses attention on the interesting high-dimensional regime where both p and N are large. The assumption is consistent with sparse designs, where for example $N = \mathcal{O}(p)$, as when we consider an increasing number of products and customers but a bounded number of ratings per customer, $\bar{n}$; it is also consistent with full designs where $N = \mathcal{O}(p^2)$, as when $n_{ij}^{(1,2)} = 1$ for all i, j, in which case $\bar{n} = \mathcal{O}(p)$; it rules out less interesting, "infill" asymptotic regimes where N grows and p is fixed, as when we get increasingly more ratings of the same products by the same customers.

To connect with the general results of Section 4.2, the vector of stacked regression coefficients $\boldsymbol{\theta}$ will be organized in $p+1$ blocks, each of which contains the level variables of a given factor, $a_i^{(k)}$. We discuss later specific orderings, but we first provide an interesting result that holds for any ordering. The proof follows easily from the lower bound in Theorem 2, see the appendix for details.

Proposition 2. *For crossed effect models with $K = 2, L = 1$, Gaussian likelihood, balanced levels and under Assumption 1,*

$$Cost(SLA) \geq \mathcal{O}(N\bar{n}).$$

Hence, contrasting this with Theorem 1, we conclude that in the high-dimensional regime we are interested in, sparse linear algebra methods have at best the same complexity as Gibbs sampling. We now consider more specific designs for which we can obtain sharper comparisons between the methods. We remain in the important special case $K = 2$, $L = 1$, and we additionally assume for simplicity that $I_1 = I_2$. Recall from Definition 2 and subsequent discussion that in this setting, and assuming balanced levels,

$\bar{n}$ is precisely the number of observations per factor level (i.e., in the recommendation analogy, the number of products rated by each customer and the number of customers rating each product). This structure leads to some progress in choosing a good ordering.

Proposition 3. *In crossed effect models with Gaussian likelihood, $K = 2$ and $L = 1$:*

(a) $n_{\boldsymbol{L}}$ is a non-increasing function of the position of $a^{(0)}$ in the ordering of $\boldsymbol{\theta}$.

(b) For the ordering $(a_1^{(1)}, \dots, a_{I_1}^{(1)}, a_1^{(2)}, \dots, a_{I_2}^{(2)}, a^{(0)})$, we have $n_{\boldsymbol{L}} = \mathcal{O}(n_{\boldsymbol{Q}} + n_{22})$, where n_{22} is the number of potential non-zeros in $\boldsymbol{L}[\boldsymbol{a}^{(2)}, \boldsymbol{a}^{(2)}]$.

Part (a) of the Proposition implies that placing $a^{(0)}$ last in the ordering of $\boldsymbol{\theta}$ is always optimal in terms of reducing $n_{\boldsymbol{L}}$, while part (b) implies that the proposed ordering leads to optimal fill-in (modulo constants) in the blocks $\boldsymbol{L}[\boldsymbol{a}^{(1)}, \boldsymbol{a}^{(1)}]$ and $\boldsymbol{L}[\boldsymbol{a}^{(1)}, \boldsymbol{a}^{(2)}]$, leaving potentially problematic fill-ins only in the block $\boldsymbol{L}[\boldsymbol{a}^{(2)}, \boldsymbol{a}^{(2)}]$. We thus employ the proposed ordering when studying the behavior of $Cost(SLA)$ in the examples below. The numerical studies we report below suggests that the orderings found by black box permutation algorithms are no better in terms of induced computational cost and fill-in ratio than the one suggested in Proposition 3. Thus, we believe that this is a good ordering for crossed effect models, and we adopt it in our analysis in the rest of this section.

The following proposition gives an example of a circulant data design with balanced levels (within the realm of Assumption 1) where sparse linear algebra complexity attains the lower bound in Proposition 2.

Proposition 4. *We consider crossed effect models with $K = 2, L = 1, I_1 = I_2 = I$, Gaussian likelihood, balanced levels, and such that $n_{ij}^{(1,2)} = 1$ when $|i - j| \leq d/2 \mod I$, for some positive even integer d, and zero otherwise. Then, $n_{\boldsymbol{L}}/n_{\boldsymbol{Q}}$ is uniformly bounded over N and d. Also, $Cost(SLA) = \mathcal{O}(N\bar{n})$, where here $\bar{n} = d + 1$, and the constants are independent of N and d.*

Even in this best-case scenario for sparse linear algebra, there is a significant difference from the complexity of Gibbs sampler in Theorem 1: in high-dimensional regimes where $\bar{n}$ (i.e., d in the design of Proposition 4) increases with N, sparse linear algebra is not scalable whereas Gibbs sampler can be due to the T_{aux} term.

The complexity of sparse linear algebra is very sensitive to the data design. In Section A.1 we describe a different structured design with balanced levels that is catastrophic for SLA. In that example $\boldsymbol{Q}$ is sparse but $\boldsymbol{L}$ is dense, more precisely $n_{\boldsymbol{Q}} = \mathcal{O}(p\bar{n})$ and $n_{\boldsymbol{L}} = \mathcal{O}(p^2)$, while

$$Cost(SLA) = \mathcal{O}(p^3) \quad \text{and} \quad Cost(Gibbs) \leq \mathcal{O}(p\bar{n}^2)\,,$$

meaning that $Cost(SLA) \gg Cost(Gibbs)$ in sparse regimes where $\bar{n} \ll p$ and that $Cost(SLA)$ is much larger than the lower bound in Proposition 2.

The previous very artificial examples are meant to illustrate two things. First, the strong sensitivity of complexity on the data design, and second, that sparse linear algebra is typically not scalable for crossed effect models whereas Gibbs sampler is. A much

more interesting research agenda is to establish theoretical results for the complexity of sparse linear algebra on interesting random designs. Here we provide a careful numerical study and defer to Section 7 a discussion on possibilities for theoretical work. We consider completely missing at random designs where each cell in the K-dimensional data contingency table contains an observation with probability π and is empty otherwise. Note that these designs do not have balanced levels. We take $I_1 = \cdots = I_K = I$, hence $N \sim Binomial(I^K, \pi)$, we consider increasing values of I, different values of K and different ways that π relates to I:
(a) $K = 2$ and $\pi = 20I^{-1}$,
(b) $K = 2$ and $\pi = I^{-1/2}$,
(c) $K = 5$ and $\pi = I^{-K+3/2}$.
The expected value of $\bar{n}$ is constant for different values of I in scenario (a), but increasing in scenarios (b) and (c). For each scenario we simulate 10 datasets, for each we numerically compute $Cost(SLA)$ and $Cost(Gibbs)$ following the definitions (17) and (9), respectively, as detailed in the Appendix, and we report the average cost for each setting. For SLA we consider both the ordering suggested in Proposition 3 and those found by the black box permutation algorithms MMD and RCM algorithms implemented in the `spam` R package.

Figure 4 reports the results, plotting the average costs versus $I\pi$, the mean value of N in each of the settings, in a log-log scale. In all three regimes, despite $\boldsymbol{Q}$ being sparse, the Cholesky factor $\boldsymbol{L}$ is dense, leading to the worst case scenario $Cost(SLA) = \mathcal{O}(p^3)$. In terms of dependence with respect to N, this leads to $Cost(SLA) = \mathcal{O}(N^3)$ in regime (a) where $N = \mathcal{O}(p)$ and $Cost(SLA) = \mathcal{O}(N^2)$ in regimes (b) and (c) where $N = \mathcal{O}(p^{3/2})$. The results confirm the intuition obtained from the previous theoretical

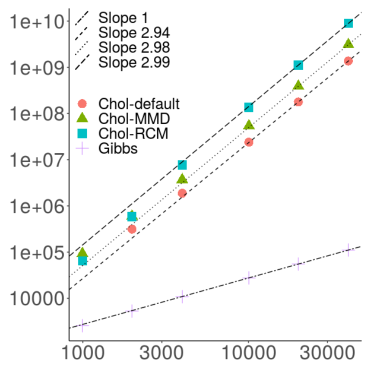

(a)

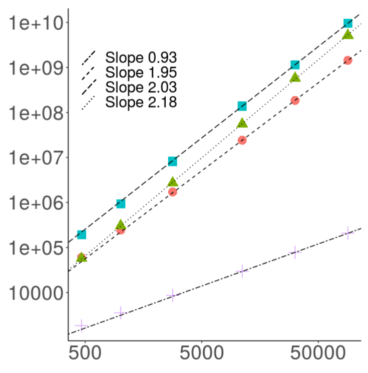

(b)

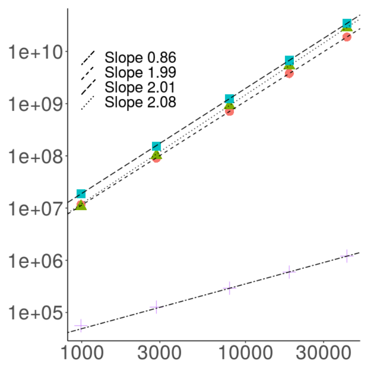

(c)

Figure 4.: Computational cost of $Cost(SLA)$ and $Cost(Gibbs)$ (y-axis) as a function of $I\pi$ (x-axis) in a log-log scale for the scenaria (a)–(c) described in the text. Each reported value is averaged over ten independent data simulations. More details in the Appendix.

analysis, according to which sparse linear algebra methods are not scalable for crossed effect models. In all cases the orderings led to similar behavior; it is interesting to report, however, that the orderings found by the black box algorithms are different from the one recommended in Proposition 4. On the contrary, we observe $Cost(Gibbs)$ growing linearly with N, which corresponds to a relaxation time that remains upper bounded or even decreases to 1 as p and N increase. Note that this behavior is consistent with the theoretical results in Section 3.2, although the setting falls outside the assumptions of Theorem 1.

4.5. Synthesis of literature

Seen as latent Gaussian models, the models we consider give rise to large sparse precision matrices. Wilkinson and Yeung (2002) and Wilkinson and Yeung (2004) show how to compute the canonical parameters of the Gaussian prior and posterior in nested multilevel models using sparse linear algebra computations and exploiting the graphical model structure to identify the zeros in the precision matrices. The potential of sparse linear algebra computations for inference and simulation in latent Gaussian models has been recognised at least since Rue (2001); this work, and inter alia the follow-ups Knorr-Held and Rue (2002) and Rue and Held (2005) have illustrated how the precision matrices that arise in spatiotemporal latent Gaussian models can be treated using sparse linear algebra algorithms, such as algorithms for banded matrices. The way numerical analysis techniques for sparse matrices can be used for computations with Gaussian graphical models is exposed in Section 2.4 of Rue and Held (2005), and Section 2.5 of the same book carries out a simulation study that tries two black-box algorithms for sparse matrices in the context of precision matrices that arise in spatiotemporal graphical models. Wilkinson and Yeung (2004) suggests sparse linear algebra methods for inference in Gaussian hierarchical models. However, the article does not study whether the structure of zeros in the precision from common families of hierarchical models is such that sparse linear algebra is efficient. These type of questions have been studied in more depth in the case of spatial models in Chapter 2 of Rue and Held (2005). In our work we pursue an analogous agenda to that in Rue and Held (2005) and establish scalability of sparse linear algebra for nested multilevel models and typically lack thereof for crossed effect models. As we discussed already in Section 3.3 our findings are very relevant to methods built around the Laplace approximation. Any such method, as for example those implemented in *lme4* and *INLA*, will work efficiently for nested multilevel models and inefficiently for crossed effect models.

5. Nested multilevel models and belief propagation

5.1. Generics on belief propagation

Belief propagation and the junction tree algorithm are two frameworks for efficient computations in graphical models. More popular within Statistics is the latter, see for example Chapter 6 of Cowell et al. (1999), and within Machine Learning the former, see for example Section 8.4 in Bishop (2006). The connections between the two paradigms are understood, see for example Chapter 2 of Wainwright and Jordan (2008). For the class of models we consider in this article the two paradigms are essentially equivalent, so we will use the belief propagation formulation, which we find more intuitive in our context and we describe below.

Belief propagation is a forward-backward algorithm for doing computations on tree-structured graphical models. The algorithm can also be used for sampling exactly posterior distributions on such graphs, as we show in this section. Belief propagation is a generalization of popular algorithms such as the Kalman filter/smoother for Gaussian state-space models, or the forward-backward algorithm for hidden Markov models (see, e.g., Chopin and Papaspiliopoulos (2020) for a description of these algorithms, and Section 5.5 below for a discussion). The starting point of belief propagation is a factorisation of the joint density of a vector of random variables. (In Section 5.2 we work with a broader framework that starts with a factorisation of the joint law of the variables, in order to account for models with non-invertible covariance matrices). The set of variables and factors are then represented by a bipartite graph known as the factor graph. There are two sets of nodes: variable nodes (one for each of the random variables) and factor nodes (one for each of the factors in the density factorisation). The edges in the graph connect each factor node to the variable nodes that correspond to those variables involved in the corresponding factor in the factorisation. Details on this construction can be found for example in Section 8.4 of Bishop (2006). For the two-level model in (4) Figure 5 shows the corresponding directed graphical model and the associated factor graph.

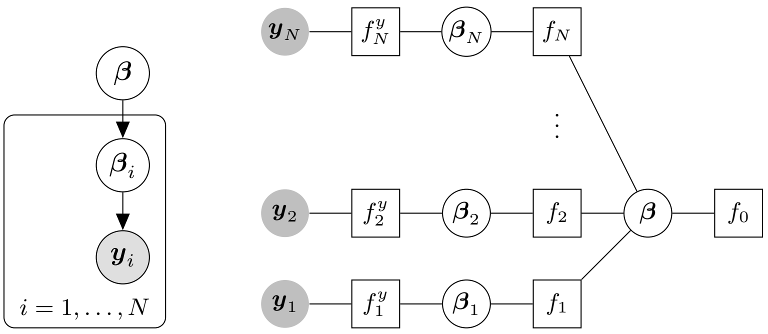

Figure 5.: Two-level hierarchical model as directed acyclic graph, aka Bayesian network (left) and as a factor graph (right). The density factorization upon which the factor graph is built is: $p(\boldsymbol{y}_{1:N}, \boldsymbol{\beta}_{1:N}, \boldsymbol{\beta}) = p(\boldsymbol{\beta}) \prod_i p(\boldsymbol{y}_i \mid \boldsymbol{\beta}_i) p(\boldsymbol{\beta}_i \mid \boldsymbol{\beta})$. The notation used for the factor nodes is explained in Section 5.2.

Belief propagation involves exchange of messages between variable and factor nodes. The messages are functions that we describe below. Let t denote a variable node in the graph, $\boldsymbol{\beta}_t$ the corresponding variable, s a neighbouring factor node, f_s the corresponding factor in the density factorisation, and $ne(\cdot)$ be a function that takes as input a node index and returns the set of neighbouring nodes in the graph. By construction factor nodes neighbour variable nodes only and variable nodes neighbour factor nodes only. Hence, f_s is a function of $\boldsymbol{\beta}_t$ and $\boldsymbol{\beta}_{ne(s)\setminus t}$. The notation is such that for sets A and B,

$A \backslash B$ denotes the set difference, we identify an element t with the one-element set that contains it, hence $A \backslash t$ is A without t, for a set of indices A, $\boldsymbol{\beta}_A$ denotes the set of variables indexed by elements in A, and $\boldsymbol{x}$ and $\boldsymbol{z}$ below denote generic function arguments, the dimensions of which vary. Messages exchanged between variable and factor nodes are functions of the variable attached to the variable node and are defined by the following equations:

$$\begin{aligned} m_{\boldsymbol{\beta}_t \to f_s}(\boldsymbol{x}) &= \prod_{k \in ne(t) \backslash s} m_{f_k \to \boldsymbol{\beta}_t}(\boldsymbol{x}) \\ m_{f_s \to \boldsymbol{\beta}_t}(\boldsymbol{z}_t) &= \int f_s(\boldsymbol{z}_{ne(s)}) \prod_{j \in ne(s) \backslash t} m_{\boldsymbol{\beta}_j \to f_s}(\boldsymbol{z}_j) d\boldsymbol{z}_j. \end{aligned} \tag{20}$$

If the factor graph is a tree, as for example in Figure 5(right), and the integrals in (20) can be computed, then the system of equations defined by (20) can be efficiently solved with a forward-backward algorithm. After choosing an arbitrary variable node as the root of the tree, we define the leaves of the tree to be the childless nodes furthest from the root. The direction from the leaves to the root is defined as forward and the reverse as backward. For a given node t, its neighbour on its unique path towards the root will be called its parent and denoted by $pa(t)$. The algorithm is initialised by setting the messages at the variables nodes at the leaves (if any) equal to 1. The forward pass of belief propagation computes messages going from the leaves to the root and the backward pass computes messages from the root to the leaves. After two sweeps we obtain the set of messages solving (20). The resulting messages can then be used to compute the marginal density at any variable node t as $p_{\boldsymbol{\beta}_t}(\boldsymbol{x}) = \prod_{s \in ne(t)} m_{f_s \to \boldsymbol{\beta}_t}(\boldsymbol{x})$. When some variables in the definition of the graphical model have been observed, say $\boldsymbol{\beta}_A$, the message passing steps that involve these variables keep them fixed at their observed values and do not integrate them out. Then, after the forward and backward steps the product of the messages at a variable node t is proportional to the conditional density $p_{\boldsymbol{\beta}_t | \boldsymbol{\beta}_A}(\boldsymbol{x})$. Although belief propagation is typically developed for computing marginal distributions and normalising constants, it can also be used to simulate from conditional distributions. This is exploited in the following section, where in the backward pass simulation replaces message computation.

5.2. Message passing for posterior sampling in nested multilevel models

We describe the messages for belief propagation in nested multilevel models as defined in (5), and how they can be used for computing $p(\boldsymbol{y} \mid \gamma)$ and simulating from $p(\boldsymbol{\theta} \mid \boldsymbol{y}, \gamma)$. The factor graph associated with (5) is a tree; throughout our presentation we will take $\boldsymbol{\beta}$ to be its root, and the $\boldsymbol{\beta}_{i_1 \ldots i_K}$ as the leaves. The factor nodes will be denoted by $f_{i_1 \ldots i_k}$. As already used in Figure 5, the factor node that links $\boldsymbol{y}_{i_1 \ldots i_k}$ to $\boldsymbol{\beta}_{i_1 \ldots i_k}$ will be denoted by $f^y_{i_1 \ldots i_k}$ and that linking $\boldsymbol{\beta}_{i_1 \ldots i_k}$ to $\boldsymbol{\beta}_{i_1 \ldots i_{k-1}}$ will be denoted by $f_{i_1 \ldots i_k}$. Messages are functions that can be parameterised in terms of a triplet $(c, \boldsymbol{C}, \boldsymbol{u})$, where c is a positive scalar, $\boldsymbol{C}$ a positive semidefinite matrix and $\boldsymbol{u}$ a vector, and for brevity we write

$$m = (c, \boldsymbol{C}, \boldsymbol{u}) \quad \text{to imply} \quad m(\boldsymbol{x}) = c \exp\left\{ -\frac{1}{2} \boldsymbol{x}^T \boldsymbol{C} \boldsymbol{x} + \boldsymbol{u}^T \boldsymbol{x} \right\}. \tag{21}$$

First we show how to update this set of parameters during the forward step. With every factor node, except those at data level, there are associated two messages, one that arrives from the variable node closer to the data and one that is sent to the variable node one level deeper. We distinguish between the two corresponding triplets by using tildes for the latter. The messages from factors at data level to the corresponding variables are

$$\begin{aligned}
m_{f^y_{i_1\dots i_k}\to\boldsymbol{\beta}_{i_1\dots i_k}} &= (\tilde{c}^y_{i_1\dots i_k}, \tilde{\boldsymbol{C}}^y_{i_1\dots i_k}, \tilde{\boldsymbol{u}}^y_{i_1\dots i_k}) \\
\tilde{\boldsymbol{C}}^y_{i_1\dots i_k} &= \tau_{i_1\dots i_k}\boldsymbol{X}^T_{i_1\dots i_k}\boldsymbol{X}_{i_1\dots i_k} \\
\tilde{c}^y_{i_1\dots i_k} &= (\tau_{i_1\dots i_k}/(2\pi))^{dim(\boldsymbol{y}_{i_1\dots i_k})/2}\exp\left\{-\frac{1}{2}\tau_{i_1\dots i_k}\boldsymbol{y}^T_{i_1\dots i_k}\boldsymbol{y}_{i_1\dots i_k}\right\} \\
\tilde{\boldsymbol{u}}^y_{i_1\dots i_k} &= \tau_{i_1\dots i_k}\boldsymbol{X}^T_{i_1\dots i_k}\boldsymbol{y}_{i_1\dots i_k}.
\end{aligned} \tag{22}$$

Notice that the message is 1 when there is no data associated to this node, i.e., when $\tau_{i_1\dots i_k} = 1$. At other levels, the factor to variable messages are

$$\begin{aligned}
m_{f_{i_1\dots i_k}\to\boldsymbol{\beta}_{i_1\dots i_{k-1}}} &= (\tilde{c}_{i_1\dots i_k}, \tilde{\boldsymbol{C}}_{i_1\dots i_k}, \tilde{\boldsymbol{u}}_{i_1\dots i_k}) \\
\tilde{c}_{i_1\dots i_k} &= c_{i_1\dots i_k}|\boldsymbol{G}|^{1/2}\exp\left\{-\frac{1}{2}\boldsymbol{u}^T_{i_1\dots i_k}\boldsymbol{\Gamma}^T\boldsymbol{G}\boldsymbol{\Gamma}\boldsymbol{u}_{i_1\dots i_k}\right\} \\
\tilde{\boldsymbol{C}}_{i_1\dots i_k} &= \boldsymbol{A}^T_{i_1\dots i_k}\boldsymbol{B}^T(\boldsymbol{B}\boldsymbol{\Sigma}_{i_1\dots i_{k-1}}\boldsymbol{B}^T+\boldsymbol{I})^{-1}\boldsymbol{B}\boldsymbol{A}_{i_1\dots i_k} \\
\tilde{\boldsymbol{u}}_{i_1\dots i_k} &= \boldsymbol{A}^T_{i_1\dots i_k}(\boldsymbol{C}_{i_1\dots i_k}\boldsymbol{\Sigma}_{i_1\dots i_{k-1}}+\boldsymbol{I})^{-1}\boldsymbol{u}_{i_1\dots i_k}
\end{aligned} \tag{23}$$

where $\boldsymbol{B}$, $\boldsymbol{\Gamma}$ and $\boldsymbol{G}$ implicitly depend on $(i_1\dots i_k)$ and are defined by

$$\boldsymbol{C}_{i_1\dots i_k} = \boldsymbol{B}^T\boldsymbol{B}, \quad \boldsymbol{\Sigma}_{i_1\dots i_{k-1}} = \boldsymbol{\Gamma}^T\boldsymbol{\Gamma}, \quad \boldsymbol{G} = (\boldsymbol{\Gamma}\boldsymbol{C}_{i_1\dots i_k}\boldsymbol{\Gamma}^T+\boldsymbol{I})^{-1}. \tag{24}$$

The triplet $(c_{i_1\dots i_k}, \boldsymbol{C}_{i_1\dots i_k}, \boldsymbol{u}_{i_1\dots i_k})$ in (23) corresponds to the message $m_{\boldsymbol{\beta}_{i_1\dots i_k}\to f_{i_1\dots i_k}}$, which is described below. The matrix decompositions in (24) are used in conjunction with Sherman-Woodbury-Morrison formula to obtain formulae that are valid without any assumptions on invertibility of either $\boldsymbol{C}_{i_1\dots i_k}$ or $\boldsymbol{\Sigma}_{i_1\dots i_k}$, since $\boldsymbol{C}_{i_1\dots i_k}\boldsymbol{\Sigma}_{i_1\dots i_{k-1}}+\boldsymbol{I}$ is invertible by construction. In the above context, the message that arrives at a variable node from above coincides with the density of the data on the leaves that originate from the given branch of the tree, conditional on the variable at this node but marginal with respect to all other variables in-between. Specifically, let $\boldsymbol{y}_{i_1\dots i_{k-1}i_k:}$ denote the set of observations that originate from $\boldsymbol{\beta}_{i_1\dots i_{k-1}i_k}$, a specific offspring of $\boldsymbol{\beta}_{i_1\dots i_{k-1}}$, then

$$\begin{aligned}
&p(\boldsymbol{y}_{i_1\dots i_{k-1}i_k:} \mid \boldsymbol{\beta}_{i_1\dots i_{k-1}}, \gamma) = \\
&\tilde{c}_{i_1\dots i_{k-1}i_k}\exp\left\{-\frac{1}{2}\boldsymbol{\beta}^T_{i_1\dots i_{k-1}}\tilde{\boldsymbol{C}}_{i_1\dots i_{k-1}i_k}\boldsymbol{\beta}_{i_1\dots i_{k-1}}+\tilde{\boldsymbol{u}}^T_{i_1\dots i_{k-1}i_k}\boldsymbol{\beta}_{i_1\dots i_{k-1}}\right\}.
\end{aligned} \tag{25}$$

The messages from variable to factor nodes are as follows:

$$m_{\boldsymbol{\beta}_{i_1\dots i_K}\to f_{i_1\dots i_K}} = (c_{i_1\dots i_K}, \boldsymbol{C}_{i_1\dots i_K}, \boldsymbol{u}_{i_1\dots i_K}) = \left(\tilde{c}^y_{i_1\dots i_K}, \tilde{\boldsymbol{C}}^y_{i_1\dots i_K}, \tilde{\boldsymbol{u}}^y_{i_1\dots i_K}\right) \tag{26}$$

while for any deeper level,

$$\begin{aligned}m_{\boldsymbol{\beta}_{i_1\dots i_k}\to f_{i_1\dots i_k}} &= (c_{i_1\dots i_k}, \boldsymbol{C}_{i_1\dots i_k}, \boldsymbol{u}_{i_1\dots i_k}) \\ &= \left(\tilde{c}^y_{i_1\dots i_k} \prod_j \tilde{c}_{i_1\dots i_k j}, \tilde{\boldsymbol{C}}^y_{i_1\dots i_k} + \sum_j \tilde{\boldsymbol{C}}_{i_1\dots i_k j}, \tilde{\boldsymbol{u}}^y_{i_1\dots i_k} + \sum_j \tilde{\boldsymbol{u}}_{i_1\dots i_k j} \right)\end{aligned} \tag{27}$$

where j runs over the appropriate index set, which depends on the numbers of offsprings $\boldsymbol{\beta}_{i_1\dots i_k}$ has on the Bayesian network.

At the root we collect messages from f_i for $i \geq 1$, which come from the level above, and from f_0, which comes from the prior. The normalised message is the posterior density at the root:

$$\begin{aligned}&\mathcal{L}(\boldsymbol{\beta} \mid \boldsymbol{y}, \boldsymbol{\gamma}) \sim \mathcal{N}(\boldsymbol{T}_{post}^{-1}\boldsymbol{\mu}_{post}, \boldsymbol{T}_{post}^{-1}) \\ &\boldsymbol{T}_{post} = \boldsymbol{T} + \boldsymbol{T}_{pr}, \quad \boldsymbol{T} = \sum_i \tilde{\boldsymbol{C}}_i \\ &\boldsymbol{\mu}_{post} = \sum_i \tilde{\boldsymbol{u}}_i + \boldsymbol{T}_{pr}\boldsymbol{\mu}_{pr}.\end{aligned} \tag{28}$$

Flat prior leads to proper posterior provided $\boldsymbol{T}$ defined above is positive definite. Additionally,

$$p(\boldsymbol{y} \mid \boldsymbol{\gamma}) = \frac{|\boldsymbol{T}_{pr}|^{1/2} \prod_i \tilde{c}_i}{|\boldsymbol{T}_{post}|^{1/2}} \exp\left\{ \frac{1}{2} (\boldsymbol{\mu}_{post}^T \boldsymbol{T}_{post}^{-1} \boldsymbol{\mu}_{post} - \boldsymbol{\mu}_{pr}^T \boldsymbol{T}_{pr} \boldsymbol{\mu}_{pr}) \right\} \tag{29}$$

where $|\boldsymbol{T}_{pr}|$ is replaced by 1 in the case of flat prior; you can directly check that this calculation follows from (25) and the definitions in (28). These calculations complete the forward pass.

For the backward pass, and for any intermediate level regression coefficients, we have

$$\begin{aligned}&\mathcal{L}(\boldsymbol{\beta}_{i_1\dots i_k} \mid \boldsymbol{\beta}_{i_1\dots i_{k-1}}, \boldsymbol{y}, \boldsymbol{\gamma}) = \\ &\mathcal{N}\left(\boldsymbol{G}(\boldsymbol{A}_{i_1\dots i_k}\boldsymbol{\beta}_{i_1\dots i_{k-1}} + \boldsymbol{\Sigma}_{i_1\dots i_{k-1}}\boldsymbol{u}_{i_1\dots i_k}), \boldsymbol{\Gamma}^T(\boldsymbol{\Gamma}\boldsymbol{C}_{i_1\dots i_k}\boldsymbol{\Gamma}^T + \boldsymbol{I})^{-1}\boldsymbol{\Gamma} \right) \\ &\boldsymbol{G} = (\boldsymbol{\Sigma}_{i_1\dots i_{k-1}}\boldsymbol{C}_{i_1\dots i_k} + \boldsymbol{I})^{-1}, \quad \boldsymbol{\Sigma}_{i_1\dots i_{k-1}} = \boldsymbol{\Gamma}^T\boldsymbol{\Gamma}.\end{aligned} \tag{30}$$

Simulating backwards according to the distributions described in (28) and (30) we obtain a draw from $p(\boldsymbol{\theta} \mid \boldsymbol{y}, \boldsymbol{\gamma})$.

We have not given the details of the calculations that produce the formulae for the messages and the conditional distributions. We have worked under a framework mathematically richer than that of (20), where the definition of a factor graph is extended to correspond to a factorisation of the joint probability measure in terms of regular conditional densities, along the lines of the disintegration theorem as in Theorem 5.4 of Kallenberg (1997). This type of construction is suitable for the factor graph representation of Bayesian networks with conditional Gaussian distributions with semi-definite covariance matrices. In the context of a multilevel model, the messages are Radon-Nikodym derivatives between Gaussian measures. It can be checked (but we have omitted the details here) that indeed the posterior Gaussian laws (30) are absolutely continuous with respect to the prior Gaussian laws in the definition of the multilevel model in (5) with Radon-Nikodym derivative proportional to the message $m_{f_{i_1\dots i_{k+1}}\to\beta_{i_1\dots i_k}}$.

5.3. Connection to sparse linear algebra

Using the connection between marginal likelihoods and the messages established in Section 5.2 and the interpretation of the Cholesky factor elements of Section 4.2, we relate the Cholesky elements to the messages exchanged in belief propagation. Note also that due to the conditional independence structure in the model,

$$p(\boldsymbol{\beta}_{i_1\dots i_k} \mid \boldsymbol{y}, \boldsymbol{\beta}_{i_1\dots i_{k-1}}, \gamma) \propto p(\boldsymbol{y}_{i_1\dots i_{k-1} i_k :} \mid \boldsymbol{\beta}_{i_1\dots i_k}, \gamma) p(\boldsymbol{\beta}_{i_1\dots i_k} \mid \boldsymbol{\beta}_{i_1\dots i_{k-1}}, \gamma),$$

for the quantities defined in (25). Therefore, we have

$$\begin{aligned} \boldsymbol{L}[\boldsymbol{\beta}_{i_1\dots i_k}, \boldsymbol{\beta}_{i_1\dots i_k}]\boldsymbol{L}[\boldsymbol{\beta}_{i_1\dots i_k}, \boldsymbol{\beta}_{i_1\dots i_k}]^T &= \boldsymbol{C}_{i_1\dots i_k} + \boldsymbol{\Sigma}^{-1}_{i_1\dots i_{k-1}} \\ \boldsymbol{L}[\boldsymbol{\beta}_{i_1\dots i_k}, \boldsymbol{\beta}_{i_1\dots i_k}]^T \boldsymbol{L}[\boldsymbol{\beta}_{i_1\dots i_k}, \boldsymbol{\beta}_{i_1\dots i_{k-1}}] &= -\boldsymbol{\Sigma}^{-1}_{i_1\dots i_{k-1}} \boldsymbol{A}_{i_1\dots i_k} \\ \boldsymbol{L}[\boldsymbol{\beta}, \boldsymbol{\beta}]\boldsymbol{L}[\boldsymbol{\beta}, \boldsymbol{\beta}]^T &= \boldsymbol{T}_{post}, \end{aligned} \tag{31}$$

where $\boldsymbol{C}_{i_1\dots i_k}$ is the matrix message as defined in (27), and $\boldsymbol{T}_{post}$ is defined in (28). A basic calculation for nested multilevel models shows that $\boldsymbol{V}\boldsymbol{m}$ is a vector of 0's except for the location that corresponds to the root, in which case it takes the value $\boldsymbol{T}_{pr}\boldsymbol{\mu}_{pr}$, thus the top equation in (10) is simplified accordingly. Working as in (31), we obtain the correspondence

$$\begin{aligned} \boldsymbol{L}[\boldsymbol{\beta}_{i_1\dots i_k}, \boldsymbol{\beta}_{i_1\dots i_k}]\boldsymbol{w}[\boldsymbol{\beta}_{i_1\dots i_k}] &= \boldsymbol{u}_{i_1\dots i_k} \\ \boldsymbol{L}[\boldsymbol{\beta}, \boldsymbol{\beta}]\boldsymbol{w}[\boldsymbol{\beta}] &= \boldsymbol{\mu}_{post}, \end{aligned} \tag{32}$$

for $\boldsymbol{u}_{i_1\dots i_k}$ the vector message as defined in (27), and $\boldsymbol{\mu}_{post}$ is defined in (28).

5.4. Complexity considerations

Both computation of $p(\boldsymbol{y} \mid \gamma)$ and the simulation from $p(\boldsymbol{\theta} \mid \boldsymbol{y}, \gamma)$ via belief propagation as described above involve a computational cost that scales linearly with N and p. The forward and backward steps at each level involve computations that without further structural assumptions scale cubically with L. On the other hand, if we wish to draw several samples for $\boldsymbol{\theta}$ for given $\boldsymbol{\gamma}$, the cost per step can be made quadratic in L, since matrix decompositions do not have to be redone. In other words, whereas the computational cost of the algorithm has the same dependence on the characteristics of the model as that of a plain vanilla Gibbs sampling algorithm that simulates each regression vector conditionally on the rest, it achieves exact draws from $p(\boldsymbol{\theta} \mid \boldsymbol{y}, \gamma)$. Sampling using belief propagation lends itself to parallelisation, but we do not develop this idea further here, although it should be considered for software development.

5.5. Synthesis of the related literature and alternative implementations

In the algorithm as described in Section 5.2, the message that arrives at a variable node from above coincides with the density of the data on the leaves that originate from the given branch of the tree, conditional on the variable at this node but marginal with respect to all other variables in-between. These messages are analogous to the so-called cost-to-go functions in state-space models (see Section 5.3.1 of Chopin and Papaspiliopoulos (2020), a terminology that originates from dynamic programming). State space models have factor graphs with single-branch tree structure. In this sense, the belief propagation as described is a generalization of an algorithm that can be used for sampling latent states in state-space models. The algorithm corresponds to a *forward* decomposition of the joint posterior $\mathcal{L}(\boldsymbol{\theta} \mid \boldsymbol{y}, \gamma)$: we first compute the messages from the data to each variable node all the way to the root, and then simulate the variables according to the *forward* transition distribution of the conditioned latent variables, $\mathcal{L}(\boldsymbol{\beta}_{i_1 \cdots i_k} \mid \boldsymbol{y}, \boldsymbol{\beta}_{i_1 \cdots i_{k-1}}, \gamma)$; see Section 5.3.1 of Chopin and Papaspiliopoulos (2020) for more details on this decomposition for state-space models and Kon Kam King et al. (2020) for a recent implementation of this idea for exact inference for of a class of non-linear state-space models. In state-space models, sampling of latent states conditionally on observations is typically done using a *backward* decomposition of the joint posterior $\mathcal{L}(\boldsymbol{\theta} \mid \boldsymbol{y}, \gamma)$, one that involves the backward transition distributions $\mathcal{L}(\boldsymbol{\beta}_{i_1 \cdots i_{k-1}} \mid \boldsymbol{y}, \boldsymbol{\beta}_{i_1 \cdots i_k}, \gamma)$, and the resultant algorithm is known as forward filtering backward sampling, see for example Algorithm 13.4 in Frühwirth-Schnatter (2006), and Sections 5.4.4 and 12.3 in Chopin and Papaspiliopoulos (2020).

The extension of Kalman filtering recursion to tree structures has been long-known, especially in the context of multiscale systems (e.g. Chou et al., 1994). Similar ideas have been exploited in spatial statistics contexts, see for example Huang and Cressie (2001) where algorithms for spatial Gaussian models with tree-structured dependence are developed. Zhang and Agarwal (2008) exploit Kalman filter recursions to perform posterior maximization for some multilevel models that are subset of the framework we consider here. These previous works typically focus on computing marginal distributions and do not develop sampling algorithms, and they do not make a clear connection with belief propagation. The connection between belief propagation and Kalman recursions is recognised in the early technical report Dempster (1990) and using a message-passing formulation in Normand and Tritchler (1992), who provide references to works even older than Dempster (1990). Note also that the connection between sparse linear algebra and Kalman filters/smoothers is discussed in Section 1.2.1 of Rue and Held (2005).

The role of belief propagation within Bayesian computation for multilevel models is fully recognised in Wilkinson and Yeung (2002) who work along the same lines we have followed in this note, in particular their Section 2.4 on message passing for sampling posteriors that arise in Gaussian tree models (the approach we use corresponds to what they call the canonical parameterisation of the multivariate Gaussian). Relative to that work the main novelty in this section is that we have worked out messages with no assumptions on invertibility of prior covariance matrices. This extension has allowed us to also cast mixed effect models as nested multilevel models and use belief propagation for those too. For the two-level mixed effect models Chib and Carlin (1999) derive an efficient algorithm for sampling the posterior distribution of the regression coefficients, which is an instance of the generic algorithm of Section 5.2, where the structure of 0's in prior covariances that results from clumping is explicitly exploited to simplify some of the matrix computations. More recently, Lindsten et al. (2016) exploit belief propagation in a multilevel hierarchical model context to integrate out Gaussian components and perform Monte Carlo inference on the remaining marginal space; see also some of the references therein for particle filters on trees.

In the opposite direction, the linear algebra community has explored the use of belief propagation as an efficient iterative method for solving linear systems. An example of this line of work is Shental et al. (2008), who use belief propagation for solving linear systems with positive definite matrices by linking the system solution to the marginal means (or the mode) of a Gaussian distribution with precision matrix given by the system matrix. They discuss connections of this approach to direct and iterative methods for solving systems and find it competitive.

6. Numerical experiments with the motivating applications

6.1. Computational methods and a comparison protocol

In this section we analyze the real estate and election survey datasets introduced in Sections 1.3 and 1.2 respectively. We approximate the posterior distributions of the corresponding nested and crossed effect models using both Monte Carlo and optimization-based methods. The Monte Carlo methods we consider are those proposed in this article, as organized in Section 2, and the *No-U-Turn Sampler* (NUTS) variant of Hamiltonian Monte Carlo of Hoffman and Gelman (2014), as implemented in *Stan* (Gelman et al., 2015). The deterministic, optimization-based method we consider is a mean-field variational Bayes approach, the *Automatic Differentiation Variational Inference* (ADVI) algorithm in Kucukelbir et al. (2017), also as implemented in *Stan*.

As it will be demonstrated, our proposed methods outperform the alternatives, often by orders of magnitude, in the sense that they deliver more accurate numerics for a given computing time. Therefore, in the numerical experiments when needed we take as "ground truth" estimates obtained through a very long run of our method (details are included in the Appendix for each of the experiments carried out). For MCMC methods, we estimate autocorrelation functions (ACFs) from a single run, where we remove the adaptation (transient) phase from the estimation. However, we plot the ACF values versus wall time (see the Appendix for more details on this). From the ACF estimates we produce an estimate of the *integrated autocorrelation time* (IAT) and *effective samples per second* (ESS/sec), as explained in Section C.2.

All simulations were carried out on a consumer machine with an Intel i5-5200 CPU and 8GB of RAM. We implemented our methods in the Python programming language and its associated scientific stack. We believe that substantial further gains in run time could be made by implementing the algorithms in a compiled language.

Details on the priors used for the two models, summary of the data structures, and additional details on the numerics (iterations, burn-in protocols, etc) are provided in the Appendix.

6.2. Results

We first compare our MCMC methods to variational inference approximations. We start our MCMC algorithms from the variational approximation at time 0 to facilitate comparisons. We compare the error in estimating posterior parameter moments as function of runtime. We monitor absolute estimation error for posterior means and posterior log standard deviations of $\boldsymbol{\theta}$ at regular time intervals, as laid out in Section C.3. This is repeated 10 times for different initializations of ADVI and different random number generators for our proposed MCMC methods. The average MCMC run outperforms the average ADVI run at any of the monitoring times. This is illustrated both in Figure 1 for the election crossed effect model and in Figure 6 for the nested multilevel real estate prices model.

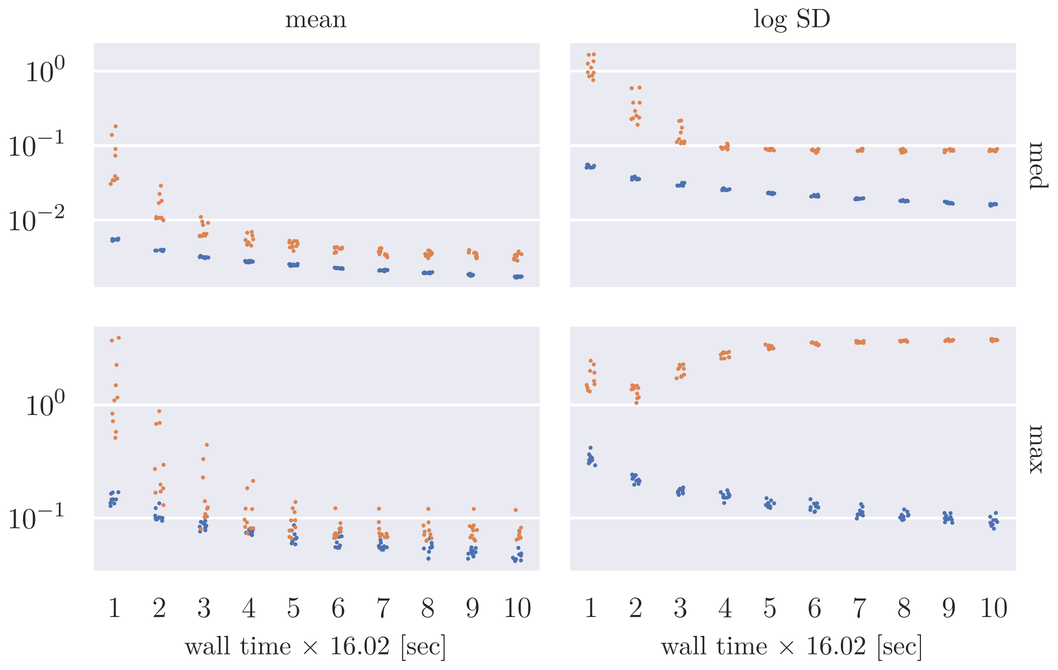

Figure 6.: *(Nested effects real estate model)* Comparison of estimation accuracy between SLA (blue) and Stan/ADVI (orange). The panels show absolute error in estimating posterior mean and log posterior standard deviation of the model coefficients ($\boldsymbol{\theta}$) as a function of run time. Each dot refers to a single run of the algorithm (there are 10 runs overall). Results are horizontally split by posterior summary and vertically by error quantile (median or max across all regression coefficients).

We subsequently compare our MCMC methods with practically relevant golden standard for Monte Carlo methods, the NUTS implementation of Hamiltonian Monte Carlo (HMC). This is a popular among practitioners algorithmic framework for a number of good reasons, including a nice software implementation through *Stan*. We estimate autocorrelation functions (ACFs) from a single run over 10000 and 1000 iterations for our methods and NUTS respectively. Where applicable, we double the length of the run to allow for adaptation and discard the first half. In both settings, our methods outperform NUTS by at least an order of magnitude in terms of effective sampling rate, and by as much as two orders of magnitude for some parameters. This has already been illustrated in Figure 2 for the nested multilevel model for real estate prices, and it can also been seen in Figure 7 for the elections crossed effect model.

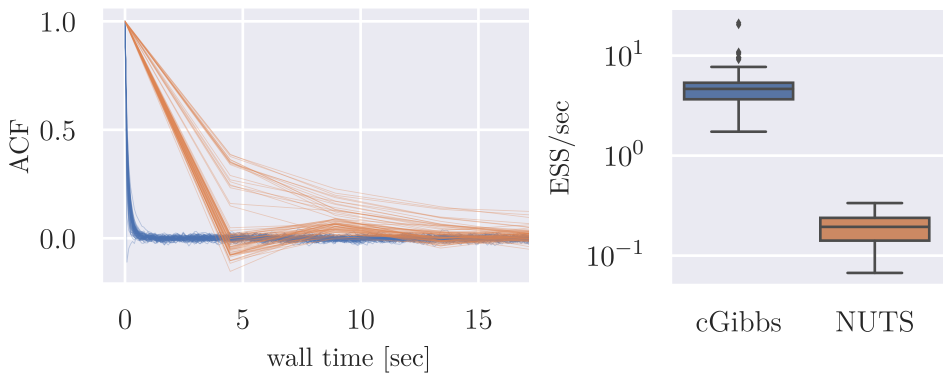

Figure 7.: *(Crossed effects elections model)* Comparison of sampling efficiency between the collapsed Gibbs sampler (blue) and Stan/NUTS (orange). The left panel overlays parameter ACFs of $\boldsymbol{\theta}$ and $\boldsymbol{\gamma}$ as a function of wall time. The right panel shows the distribution of effective samples per second.

Detailed numerical comparisons between our MCMC methods and Stan/NUTS are given in tables 2 and 3 for the nested multilevel model and in tables 4 and 5 for the crossed effects model.

7. Beyond

In this section we collect a number of ideas we are currently exploring and pointers to open problems.

7.1. Non-Gaussian nested models

The article has not proposed a framework for scalable computation for nested multilevel models with non-Gaussian likelihoods. An obvious approach is to use a gradient-based sampler that exploits the structured prior for preconditioning and the sparsity in the prior precision to obtain $\mathcal{O}(1)$ computational cost per iteration. We have worked out such an algorithm, built around that in Titsias and Papaspiliopoulos (2018), but it will rarely be the case that any such sampler will have $\mathcal{O}(1)$ relaxation time, thus even if practically relevant it will be outside the scope defined in this paper. A promising alternative, when there are data available only at the highest level as in the application of Section 6, is

k	algorithm	$\boldsymbol{\theta}$			$\boldsymbol{\gamma}$
		max	med	min	
0	SLA	12.52	12.29	12.07	10.10
	Stan/NUTS	0.23	0.13	0.04	0.19
1	SLA	13.98	12.41	10.57	6.29
	Stan/NUTS	0.79	0.42	0.13	0.28
2	SLA	14.71	12.59	10.63	4.23
	Stan/NUTS	1.00	0.49	0.22	0.22
3	SLA	14.44	12.58	10.24	3.47
	Stan/NUTS	0.94	0.49	0.21	0.16
4	SLA	14.61	12.58	10.56	-
	Stan/NUTS	0.86	0.39	0.17	-

Table 2.: (*Nested effects real estate model*) We estimate effective sample size per second for elements of $\boldsymbol{\theta}$ and traces of elements of $\boldsymbol{\gamma}$, and report summary statistics by level k.

algorithm	$\boldsymbol{\theta}$			$\boldsymbol{\gamma}$	iteration time	integration steps
	max	med	min	med	mean	mean
SLA	14.71	12.58	10.24	5.26	0.08	-
Stan/NUTS	1.00	0.45	0.04	0.20	3.97	255

Table 3.: (*Nested effects real estate model*) We estimate effective sample size per second for elements of $\boldsymbol{\theta}$ and traces of elements of $\boldsymbol{\gamma}$, and report summary statistics.

k	algorithm	$\boldsymbol{\theta}$			$\boldsymbol{\gamma}$
		max	med	min	
0	cGibbs	21.25	20.79	20.33	-
	Stan/NUTS	0.18	0.16	0.15	-
1	cGibbs	7.71	6.46	5.47	10.89
	Stan/NUTS	0.09	0.08	0.07	0.19
2	cGibbs	5.43	5.14	4.34	9.53
	Stan/NUTS	0.12	0.11	0.09	0.18
3	cGibbs	5.30	4.38	3.49	9.39
	Stan/NUTS	0.14	0.13	0.12	0.23
4	cGibbs	4.85	4.39	3.91	9.56
	Stan/NUTS	0.12	0.11	0.10	0.19
5	cGibbs	6.02	5.48	5.09	10.67
	Stan/NUTS	0.13	0.10	0.07	0.19
6	cGibbs	10.37	4.35	1.73	2.31
	Stan/NUTS	0.34	0.22	0.12	0.13
7	cGibbs	3.71	3.39	3.08	9.62
	Stan/NUTS	0.11	0.10	0.09	0.19

Table 4.: (*Crossed effects elections model*) We estimate effective sample size per second for elements of $\boldsymbol{\theta}$ and traces of elements of $\boldsymbol{\gamma}$, and report summary statistics by factor k.

algorithm	$\boldsymbol{\theta}$			$\boldsymbol{\gamma}$	iteration time	integration steps
	max	med	min	med	mean	mean
cGibbs	21.25	4.58	1.73	9.56	0.08	-
Stan/NUTS	0.34	0.20	0.07	0.19	4.46	334.35

Table 5.: (*Crossed effects elections model*) We estimate effective sample size per second for all for elements of $\boldsymbol{\theta}$ and traces of elements of $\boldsymbol{\gamma}$, and report summary statistics.

to block $\boldsymbol{\theta} = (\boldsymbol{\theta}_l, \boldsymbol{\theta}_b)$, for $\boldsymbol{\theta}_l$ the parameters on the leaves linked to the data and $\boldsymbol{\theta}_b$ the remaining ones. Sampling $\mathcal{L}(\boldsymbol{\theta}_b \mid \boldsymbol{y}, \boldsymbol{\theta}_l, \boldsymbol{\gamma}) = \mathcal{L}(\boldsymbol{\theta}_b \mid \boldsymbol{\theta}_l, \boldsymbol{\gamma})$ is done as we have discussed in this article, by belief propagation or sparse linear algebra, with $\boldsymbol{\theta}_l$ playing the role of $\boldsymbol{y}$. Sampling $\mathcal{L}(\boldsymbol{\theta}_l \mid \boldsymbol{y}, \boldsymbol{\theta}_b, \boldsymbol{\gamma})$ can be done efficiently since the target factorizes into conditionally independent L-dimensional distributions. The issue with this approach is the posterior dependence between $\boldsymbol{\theta}_l$ and $\boldsymbol{\theta}_b$. From the work in Papaspiliopoulos and Roberts (2008) for models with $K = 2$ and single-branch structure we know that the stability of Gibbs sampling algorithms for sampling $\mathcal{L}(\boldsymbol{\theta}_l, \boldsymbol{\theta}_b \mid \boldsymbol{y}, \boldsymbol{\gamma})$ critically depends on the tails of the observation density. This theory is not available yet for general K and multi-branch structures, but we are making progress in this direction.

7.2. Provable scalability for the full sampler

Following the discussion in Section 2, we have focused on providing provably scalable algorithms to sample from $\mathcal{L}(\boldsymbol{\theta} \mid \boldsymbol{y}, \boldsymbol{\gamma})$. Extensive numerical simulations, both in this paper and in related work, suggest that efficient updates of $\mathcal{L}(\boldsymbol{\theta} \mid \boldsymbol{y}, \boldsymbol{\gamma})$ are sufficient to ensure good performance for the full scheme that alternates the updates from $\mathcal{L}(\boldsymbol{\theta} \mid \boldsymbol{y}, \boldsymbol{\gamma})$ and $\mathcal{L}(\boldsymbol{\gamma} \mid \boldsymbol{y}, \boldsymbol{\theta})$. We have discussed upper bounds on the relaxation times of the conditional updates, $\mathcal{L}(\boldsymbol{\theta} \mid \boldsymbol{y}, \boldsymbol{\gamma})$, that are uniform with respect to N and p in many regimes of interest. Note that these bounds are not uniform with respect to $\boldsymbol{\gamma}$, for example the upper bounds in the proof of Theorem 1 diverge when τ_1 and τ_2 go to 0. While this will not create computational issues in regimes where the posterior concentrates away of that region, it suggests that employing informed priors to reduce the posterior mass in those corners of the parameter space, which are computationally problematic but statistically not crucial, may be beneficial in terms of computational robustness. We are currently working on deriving explicit convergence results for the full sampler. We seek to prove that, under appropriate assumptions on the data generating mechanism and on the algorithm's initialization, the mixing time of the full sampler remains bounded as N and p diverge to infinity, with K fixed. The approach is asymptotic in nature, since it relies on the asymptotic normality of the marginal posterior distribution of the fixed-dimensional hyperparameters, $\mathcal{L}(\boldsymbol{\gamma} \mid \boldsymbol{y})$. Other approaches are currently being developed for related problems, see e.g. Jin and Hobert (2021) and references therein.

7.3. Jointly nested and crossed effect models

Hierarchical models with both nested and crossed random effects are common in applications. Returning to our motivating toy recommender system example, consider customers i organized within groups k rating products j, with the linear predictor $\eta_{kij} = \beta_{ki} + a_j$, product random effects $a_j \sim \mathcal{N}(0, \tau_p^{-1})$, customer effects $\beta_{ki} \sim \mathcal{N}(\beta_k, \tau_c^{-1})$, and group effects $\beta_k \sim \mathcal{N}(\mu, \tau_g^{-1})$ (where we have adapted the notation to be more functional within this mixed framework). We can combine belief propagation and collapsed Gibbs sampling to obtain efficient methods in this context, the intuition being that we can leverage the former to update efficiently the tree-structured random effects from their conditional distribution, and the latter to define blocks of effects to be jointly sampled.

With Gaussian likelihood we can extend our complexity theory in such contexts.

7.4. Random graphs, weak dependence and complexity

Theorem 1 provides an insightful connection between the relaxation time of the collapsed Gibbs sampler targeting $\mathcal{L}(\boldsymbol{\theta} \mid \boldsymbol{y}, \gamma)$ and the relaxation time T_{aux} of an auxiliary random walk on the conditional independence graph of $\boldsymbol{\theta}$ (this random walk is stochastically equivalent to the Gibbs sampler described in the section). This result opens up to interesting and unexplored connections between the Bayesian computation literature and the literature about random walks on (random) graphs. For instance, variations of Friedman's second eigenvalue Theorem (Bordenave, 2019) can be used to establish that the relaxation time T_{aux} defined in Theorem 1 remains upper bounded under as N and p diverge under data missing at random assumptions. We are currently using such results to derive rigorous statements about the complexity of sampling algorithms for $\mathcal{L}(\boldsymbol{\theta} \mid \boldsymbol{y}, \gamma)$. Also, it would be interesting to extend Theorem 1 in many directions, such as considering $K > 2$ or unbalanced designs. Both such extensions are non-trivial and would lead to a significant generalization of the result. In order to consider unbalanced designs, one needs to extend proof techniques based on multigrid decompositions (Zanella and Roberts, 2020; Papaspiliopoulos et al., 2020), which exploit the exact independence between appropriate reparametrizations of $\boldsymbol{\theta}$, to cases of weak dependence. In this direction, the proof strategy of Ghosh et al. (2020) can be interesting, which exploits appropriate concentration inequalities to provide upper bounds on the convergence rate of coordinate-wise optimization for computing the MAP estimator for crossed effects with unbalanced levels.

7.5. Approximate sparse linear algebra

Conditional independence graphs of $\boldsymbol{\theta}$ with good connectivity properties, such as random and unstructured graphs, lead to fast mixing of the collapsed Gibbs Sampler. Sparse linear algebra performs very well on structured designs, such as spatial grids or near-banded designs (see e.g. Proposition 4), while it suffers with unstructured and random designs (see Section 4.4 and Figure 4). This renders sparse linear algebra methods inappropriate for crossed effect models. While this is true for *exact* sparse linear algebra methods, we expect a very different picture to hold for approximate ones. Indeed, most entries in the Cholesky factors $\boldsymbol{L}$ arising from crossed models are very close to 0, and do not contribute significantly when reconstructing $\boldsymbol{Q}$ as $\boldsymbol{L}\boldsymbol{L}^T$. Thus, a sparse approximation to $\boldsymbol{L}$ is sufficient for the purpose of sampling from $\mathcal{L}(\boldsymbol{\theta} \mid \boldsymbol{y}, \gamma)$. To illustrate the point, we construct a sparse approximate Cholesky factor $\tilde{\boldsymbol{L}}$ by simply thresholding elements in the original factor $\boldsymbol{L}$. Figure 8 displays the resulting relative error in Frobenius norm when reconstructing $\boldsymbol{Q}$, i.e. $\|\boldsymbol{Q} - \tilde{\boldsymbol{L}}\tilde{\boldsymbol{L}}^T\|_F / \|\boldsymbol{Q}\|_F$, as a function of the proportion of thresholded values for the worst case design of Section A.1 with $\bar{n} = 4$. We can see that, if one allows a relative error of 10^{-6}, about 99% of the values in $\boldsymbol{L}$ can be set to 0 when $I = 5000$, and that the fraction of negligible values increases with I. There are way more sophisticated and computationally scalable ways to produce

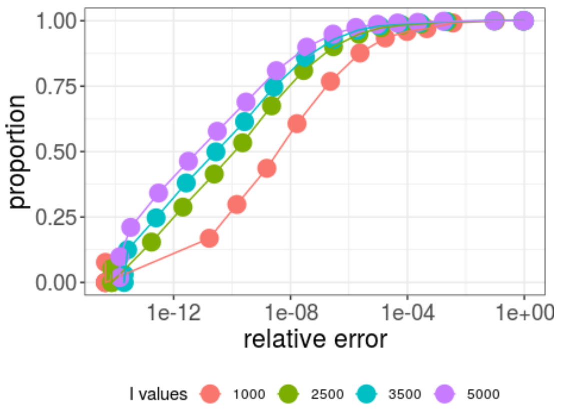

Figure 8.: Relative error in Frobenius norm for reconstructing $\boldsymbol{Q}$ as a function of the proportion of thresholded values in $\boldsymbol{L}$, for the design of Section A.1 with $\bar{n} = 4$ and different values of I.

sparse approximations than thresholding, and they will not require precomputing $\boldsymbol{L}$. For example, see Schäfer et al., 2020 (and references therein) for methods based on covariance matrices built by kernels. There can be devised schemes based instead on precision matrices and tailored to the crossed effect structure, which we report in future work. Embedding approximate linear algebra methods within sampling algorithms naturally relates to recent work on theoretical guarantees for approximate MCMC methods (Rudolf et al., 2018), see e.g. Johndrow et al. (2020) for an application to sparse regression models.

Acknowledgements

The development of belief propagation for nested multilevel models first appeared in the unpublished technical report Papaspiliopoulos and Zanella (2017) by two of the authors. The authors are most grateful for their inputs Mr Jie Hao Kwa, whose master dissertation in 2018 obtained useful insights into sparse linear algebra methods for nested multilevel models, and Maximilan Müller, whose master dissertation in 2020 investigated sparse linear methods for crossed effect models and proposed the worst-case design in Section A.1. The first two authors would like to thank Jose Garcia-Montalvo for the collaboration on the applied projects that have motivated this work. The article has benefited from comments by Darren Wilkinson.

References

Andrieu, C. and Thoms, J. (2008). A tutorial on adaptive mcmc. *Statistics and computing*, 18(4):343–373.

Bates, D., Mächler, M., Bolker, B., and Walker, S. (2015). Fitting linear mixed-effects models using lme4. *Journal of Statistical Software*, 67(1):1–48.

Bishop, C. M. (2006). *Pattern recognition and machine learning.* Information Science and Statistics. Springer, New York.

Bordenave, C. (2019). A new proof of friedman's second eigenvalue theorem and its extension to random lifts. In *Annales scientifiques de l'Ecole normale supérieure.*

Chib, S. and Carlin, B. P. (1999). On mcmc sampling in hierarchical longitudinal models. *Statistics and Computing*, (9):17–26.

Chopin, N. and Papaspiliopoulos, O. (2020). *An Introduction to Sequential Monte Carlo.* Springer.

Chou, K. C., Willsky, A. S., and Nikoukhah, R. (1994). Multiscale systems, Kalman filters, and Riccati equations. *IEEE Transactions on Automatic Control*, 39(3):479–492.

Cowell, R. G., Dawid, A. P., Lauritzen, S. L., and Spiegelhalter, D. J. (1999). *Probabilistic networks and expert systems.* Statistics for Engineering and Information Science. Springer-Verlag, New York.

Dempster, A. (1990). Normal belief functions and the kalman filter.

Frühwirth-Schnatter, S. (2006). *Finite mixture and Markov switching models.* Springer Series in Statistics. Springer, New York.

Gao, K. and Owen, A. (2017). Efficient moment calculations for variance components in large unbalanced crossed random effects models. *Electronic Journal of Statistics*, 11(1):1235–1296.

Gao, K. and Owen, A. B. (2020). Estimation and inference for very large linear mixed effects models. *Statistica Sinica*, 30:1741–1771.

Gelfand, A. E., Sahu, S. K., and Carlin, B. P. (1996). Efficient parametrizations for generalized linear mixed models. In *Bayesian statistics, 5 (Alicante, 1994)*, Oxford Sci. Publ., pages 165–180. Oxford Univ. Press, New York.

Gelman, A. (2005). Analysis of variance: why it is more important than ever. *The Annals of Statistics*, 33(1):1–53.

Gelman, A. and Hill, J. (2007). *Data analysis using regression and multilevel/hierarchical models*, volume 3. Cambridge University Press New York, New York, USA.

Gelman, A., Lee, D., and Guo, J. (2015). Stan: A probabilistic programming language for bayesian inference and optimization. *Journal of Educational and Behavioral Statistics*, 40(5):530–543.

Ghosh, S., Hastie, T., and Owen, A. B. (2020). Backfitting for large scale crossed random effects regressions. *arXiv preprint arXiv:2007.10612*.

Gilbert, J. R. (1994). Predicting structure in sparse matrix computations. *SIAM Journal on Matrix Analysis and Applications*, 15(1):62–79.

Golub, G. H. and van Loan, C. F. (2013). *Matrix Computations*. JHU Press, fourth edition.

Goplerud, M. (2020). Fast and accurate estimation of non-nested binomial hierarchical models using variational inference. *arXiv preprint arXiv:2007.12300*.

Hoffman, M. D. and Gelman, A. (2014). The no-u-turn sampler: adaptively setting path lengths in hamiltonian monte carlo. *J. Mach. Learn. Res.*, 15(1):1593–1623.

Huang, H.-C. and Cressie, N. (2001). Multiscale graphical modeling in space: applications to command and control. In *Spatial statistics: methodological aspects and applications*, volume 159 of *Lect. Notes Stat.*, pages 83–113. Springer, New York.

Jin, Z. and Hobert, J. P. (2021). Dimension free convergence rates for Gibbs samplers for Bayesian linear mixed models. *arXiv preprint arXiv:2103.06324*.

Johndrow, J. E., Orenstein, P., and Bhattacharya, A. (2020). Scalable Approximate MCMC Algorithms for the Horseshoe Prior. *Journal of Machine Learning Research*, 21(73):1–61.

Kallenberg, O. (1997). *Foundations of modern probability*. Probability and its Applications (New York). Springer-Verlag, New York.

Knorr-Held, L. and Rue, H. v. (2002). On block updating in Markov random field models for disease mapping. *Scand. J. Statist.*, 29(4):597–614.

Kon Kam King, G., Papaspiliopoulos, O., and Ruggiero, M. (2020). Exact inference for a class of non-linear hidden markov models on general state spaces.

Kucukelbir, A., Tran, D., Ranganath, R., Gelman, A., and Blei, D. M. (2017). Automatic differentiation variational inference. *The Journal of Machine Learning Research*, 18(1):430–474.

Lindsten, F., Johansen, A. M., Naesseth, C. A., Kirkpatrick, B., Schön, T. B., Aston, J., and Bouchard-Côté, A. (2016). Divide-and-conquer with sequential monte carlo. *Journal of Computational and Graphical Statistics*, (In press).

Liu, J. S. and Wu, Y. N. (1999). Parameter expansion for data augmentation. *Journal of the American Statistical Association*, 94(448):1264–1274.

Meng, X.-L. and Van Dyk, D. A. (1999). Seeking efficient data augmentation schemes via conditional and marginal augmentation. *Biometrika*, 86(2):301–320.

Menictas, M., Di Credico, G., and Wand, M. P. (2019). Streamlined variational inference for linear mixed models with crossed random effects. *arXiv preprint arXiv:1910.01799*.

Montalvo, J. G., Papaspiliopoulos, O., and Stumpf-Fétizon, T. (2019). Bayesian forecasting of electoral outcomes with new parties' competition. *European Journal of Political Economy*, 59:52–70.

Normand, S.-L. and Tritchler, D. (1992). Parameter updating in a Bayes network. *Journal of the American Statistical Association*, 87(420):1109–1115.

Papaspiliopoulos, O. and Roberts, G. (2008). Stability of the Gibbs sampler for Bayesian hierarchical models. *The Annals of Statistics*, 36(1):95 – 117.

Papaspiliopoulos, O., Roberts, G., and Zanella, G. (2020). Scalable inference for crossed random effect models. *Biometrika*, (107):24–40.

Papaspiliopoulos, O., Roberts, G. O., and Sköld, M. (2007). A general framework for the parametrization of hierarchical models. *Statist. Sci.*, 22(1):59–73.

Papaspiliopoulos, O. and Zanella, G. (2017). A note on mcmc for nested multilevel regression models via belief propagation.

Perry, P. O. (2016). Fast moment-based estimation for hierarchical models. *Journal of the Royal Statistical Society: Series B (Statistical Methodology)*, 79(1):267–291.

Rivin, I. (2002). Counting cycles and finite dimensional lp norms. *Advances in Applied Mathematics*, 29(4):647 – 662.

Roberts, G. O. and Sahu, S. K. (1997). Updating schemes, correlation structure, blocking and parameterization for the gibbs sampler. *Journal of the Royal Statistical Society: Series B (Statistical Methodology)*, 59(2):291–317.

Rosenthal, J. S. (2003). Asymptotic variance and convergence rates of nearly-periodic markov chain monte carlo algorithms. *Journal of the American Statistical Association*, 98(461):169–177.

Rudolf, D., Schweizer, N., et al. (2018). Perturbation theory for Markov chains via Wasserstein distance. *Bernoulli*, 24(4A):2610–2639.

Rue, H. and Held, L. (2005). *Gaussian Markov random fields: theory and applications*. Chapman & Hall.

Rue, H., Martino, S., and Chopin, N. (2009). Approximate bayesian inference for latent gaussian models by using integrated nested laplace approximations. *Journal of the royal statistical society: Series b (statistical methodology)*, 71(2):319–392.

Rue, H. v. (2001). Fast sampling of Gaussian Markov random fields. *J. R. Stat. Soc. Ser. B Stat. Methodol.*, 63(2):325–338.

Schäfer, F., Katzfuss, M., and Owhadi, H. (2020). Sparse cholesky factorization by kullback-leibler minimization. *arXiv preprint arXiv:2004.14455*.

Searle, S. R., Casella, G., and McCulloch, C. E. (2009). *Variance components*, volume 391. John Wiley & Sons.

Shental, O., Bickson, D., Siegel, P. H., Wolf, J. K., and Dolev, D. (2008). Gaussian belief propagation solver for systems of linear equations. In *EEE Int. Symp. on Inform. Theory (ISIT)*.

Sokal, A. (1997). Monte carlo methods in statistical mechanics: foundations and new algorithms. In *Functional integration*, pages 131–192. Springer.

Titsias, M. K. and Papaspiliopoulos, O. (2018). Auxiliary gradient-based sampling algorithms. *Journal of the Royal Statistical Society Series B*, 80(4):749–767.

Vallejos, C. A., Marioni, J. C., and Richardson, S. (2015). BASiCS: Bayesian analysis of single-cell sequencing data. *PLoS Comput Biol*, 11(6):e1004333.

Vines, S., Gilks, W., and Wild, P. (1996). Fitting Bayesian multiple random effects models. *Statistics and Computing*, 6(4):337–346.

Volfovsky, A. and Hoff, P. D. (2014). Hierarchical array priors for ANOVA decompositions of cross-classified data. *Ann. Appl. Stat.*, 8(1):19–47.

Wainwright, M. J. and Jordan, M. I. (2008). Graphical models, exponential families, and variational inference. *Foundations and Trends in Machine Learning*, 1(1-2):1–305.

Wilkinson, D. J. and Yeung, S. K. H. (2002). Conditional simulation from highly structured Gaussian systems, with application to blocking-MCMC for the Bayesian analysis of very large linear models. *Stat. Comput.*, 12(3):287–300.

Wilkinson, D. J. and Yeung, S. K. H. (2004). A sparse matrix approach to Bayesian computation in large linear models. *Comput. Statist. Data Anal.*, 44(3):493–516.

Zanella, G. and Roberts, G. (2020). Multilevel linear models, Gibbs samplers and multigrid decompositions. *Bayesian Analysis*.

Zhang, L. and Agarwal, D. (2008). Fast computation of posterior mode in multi-level hierarchical models. In Koller, D., Schuurmans, D., Bengio, Y., and Bottou, L., editors, *Advances in Neural Information Processing Systems 21*, pages 1913–1920.

A. Proofs

Proof of Theorem 1. The cost per iteration has been established to be $\mathcal{O}(2N + p)$, hence the proof focuses on quantifying the relaxation time. Denote by T_{cgs} the relaxation time of the collapsed Gibbs sampler applied to $\mathcal{L}(\boldsymbol{\theta} \mid \boldsymbol{y}, \boldsymbol{\gamma})$. We now prove that

$$c \min\{\bar{n}, T_{aux}\} \leq T_{cgs} \leq C \min\{\bar{n}, T_{aux}\} \tag{33}$$

for any balanced level design and for some positive and finite constants c and C, which depend only on $\boldsymbol{\gamma}$. The thesis follows directly from (33) and the fact that the cost per iteration of the Gibbs Sampler is $\mathcal{O}(N)$.

By Papaspiliopoulos et al. (2020, Theorem 4) we have $T_{cgs} = (1 - \rho_1\rho_2\rho_{aux})^{-1}$ where $\rho_k = (N\tau + I_k\tau_k)^{-1}N\tau$ for $k = 1, 2$, ρ_{aux} is the L^2-rate of convergence of the auxiliary Gibbs sampler satisfying $T_{aux} = (1 - \rho_{aux})^{-1}$, τ is the likelihood precision and τ_k the prior precision of the k-th factor. Since $\rho \mapsto (1 - \rho)^{-1}$ is increasing on $(0, 1)$ and $\rho_1\rho_2\rho_{aux} \leq \min\{\rho_1, \rho_2, \rho_{aux}\}$, it follows

$$T_{cgs} \leq (1 - \min\{\rho_1, \rho_2, \rho_{aux}\})^{-1} = \min\left\{(1 - \min\{\rho_1, \rho_2\})^{-1}, (1 - \rho_{aux})^{-1}\right\} .$$

By definition of ρ_1 and ρ_2 it follows

$$(1 - \min\{\rho_1, \rho_2\})^{-1} = 1 + \frac{N\tau}{\max\{I_1\tau_1, I_2\tau_2\}} \leq 1 + C_1\frac{N}{\max\{I_1, I_2\}} \leq 1 + C_1\bar{n}\,, \tag{34}$$

with $C_1 = \frac{\tau}{\min\{\tau_1,\tau_2\}}$ and exploiting $\max\{I_1, I_2\} \geq 2^{-1}(I_1 + I_2)$. Combining the above inequalities with $T_{aux} = (1 - \rho_{aux})^{-1}$ we obtain

$$T_{cgs} \leq \min\{1 + C_1\bar{n}, T_{aux}\} \leq C\min\{\bar{n}, T_{aux}\}\ ,$$

where we can take $C = 1 + C_1$ since $\bar{n} \geq 1$ by construction.

For the lower bound, $\rho_1\rho_2\rho_{aux} \geq (\min\{\rho_1, \rho_2, \rho_{aux}\})^3$ implies

$$T_{cgs} \geq (1 - \min\{\rho_1, \rho_2, \rho_{aux}\}^3)^{-1} \geq 3^{-1}(1 - \min\{\rho_1, \rho_2, \rho_{aux}\})^{-1}\,,$$

where the second inequality follows from $(1 - \rho^t)^{-1} \geq t^{-1}(1 - \rho)^{-1}$ for every $t \geq 1$ and $\rho \in (0, 1)$. To prove the latter claim note that $(1 - \rho^t)^{-1} \geq t^{-1}(1 - \rho)^{-1}$ if and only if $\rho^t - t\rho + (t - 1) \geq 0$ and that the left-hand side is a decreasing function of ρ on $(0, 1)$ that vanishes when $\rho = 0$. It follows that

$$T_{cgs} \geq 3^{-1}\min\left\{(1 - \min\{\rho_1, \rho_2\})^{-1}, (1 - \rho_{aux})^{-1}\right\} .$$

Then, analogously to (34), we have

$$(1 - \min\{\rho_1, \rho_2\})^{-1} \geq \frac{N\tau}{\max\{I_1\tau_1, I_2\tau_2\}} \geq c_1\frac{N}{\max\{I_1, I_2\}} \geq \frac{c_1}{2}\bar{n}\,,$$

with $c_1 = \frac{\tau}{\max\{\tau_1,\tau_2\}}$ and exploiting $\max\{I_1, I_2\} \leq (I_1 + I_2)$. Thus, we obtain

$$T_{cgs} \geq \min\left\{\frac{c_1}{2}\bar{n}, T_{aux}\right\} \geq c\min\{\bar{n}, T_{aux}\}$$

with $c = \min\{1, \frac{c_1}{2}\}$, as desired. □

Proof of Theorem 2. The recursive equations in (15) can be solved through the following algorithm:
1) Set $\boldsymbol{L}_{11} = Chol(\boldsymbol{Q}_{11})$ and $\boldsymbol{L}_{j1} = \boldsymbol{L}_{11}^{-1}\boldsymbol{Q}_{j1}$ for $j = 2, \ldots, M$
2) For $m = 2, \ldots, M$ do:

- Set $\boldsymbol{L}_{mm} = Chol(\boldsymbol{Q}_{mm} - \sum_{\ell=1}^{m-1} \boldsymbol{L}_{m\ell}\boldsymbol{L}_{m\ell}^T)$
- For $j = m+1, \dots, M$, set $\boldsymbol{L}_{jm} = \boldsymbol{L}_{mm}^{-1}(\boldsymbol{Q}_{jm} - \sum_{\ell=1}^{m-1} \boldsymbol{L}_{m\ell}\boldsymbol{L}_{j\ell})$,

where we assume to be able to decompose and invert L-dimensional matrices within each block. When $L = 1$, counting the number of operations required by the above algorithm we obtain that

$$Cost(SLA) = \sum_{m=1}^{M} 1 + n_{\boldsymbol{L},m} + n_{\boldsymbol{L},m}(1 + n_{\boldsymbol{L},m}), \tag{35}$$

see also Theorem 2.2 of https://www.tau.ac.il/~stoledo/Support/chapter-direct.pdf for a step-by-step derivation of (35). When L is larger than 1 but fixed, one gets additional multiplicative constant in (35). In both cases we have $Cost(SLA) = \mathcal{O}\left(\sum_{m=1}^{M} n_{\boldsymbol{L},m}^2\right)$ as stated in (17).

Then, using Jensen inequality and $\sum_{m=1}^{M} n_{\boldsymbol{L},m} = n_{\boldsymbol{L}}$ we have

$$\sum_{m=1}^{M} n_{\boldsymbol{L},m}^2 = M\left(M^{-1}\sum_{m=1}^{M} n_{\boldsymbol{L},m}^2\right) \geq M\left(M^{-1}\sum_{m=1}^{M} n_{\boldsymbol{L},m}\right)^2 = n_{\boldsymbol{L}}^2/M,$$

which proves the lower bound in (17).

The upper bound in (17), instead, cannot be deduced purely from $Cost(SLA) = \mathcal{O}\left(\sum_{m=1}^{M} n_{\boldsymbol{L},m}^2\right)$, but rather it follows from a characterization of $Cost(SLA)$ in terms of 3-cycles of an undirected graph associated to $\boldsymbol{L}$. More precisely, define $G_{\boldsymbol{L}}$ as the undirected graph with nodes $\{1, \dots, M\}$ and an edge between vertices $j > m$ if and only if the future set of $\boldsymbol{\theta}_m$ does not separate it from $\boldsymbol{\theta}_j$ in $G_{\boldsymbol{Q}}$. For any $j, m \in \{1, \dots, M\}$ with $j \neq m$, we write $\{j, m\} \in G_{\boldsymbol{L}}$ if there is an edge between j and m in $G_{\boldsymbol{L}}$. By the arguments in Section 4.2, $\boldsymbol{L}_{j\ell}$ is (a potential) non-zero if and only if $\{j, \ell\} \in G_{\boldsymbol{L}}$. The dominating cost in the algorithm discussed above to obtain $\boldsymbol{L}$ is the computation of $\sum_{\ell=1}^{m-1} \boldsymbol{L}_{m\ell}\boldsymbol{L}_{j\ell}$ for $m = 2, \dots, M$ and $j = m+1, \dots, M$. Ignoring multiplications by zero and summation of zeros, this corresponds to

$$\mathcal{O}(|\{(\ell, m, j) : \{m, \ell\} \in G_{\boldsymbol{L}}, \{j, \ell\} \in G_{\boldsymbol{L}} \text{ and } 1 \leq \ell < m < j \leq M\}|) \tag{36}$$

operations. By definition of $G_{\boldsymbol{L}}$, if $\{\ell, m\} \in G_{\boldsymbol{L}}$ and $\{\ell, j\} \in G_{\boldsymbol{L}}$ for $\ell < m < j$, then also $\{\ell, m\} \in G_{\boldsymbol{L}}$. Thus, the cost in (36) coincides with the number of 3-cycles in $G_{\boldsymbol{L}}$. The upper bound in (17) then follows noting that the number of 3-cycles in an undirected graph with $n_{\boldsymbol{L}}$ edges is less or equal than $n_{\boldsymbol{L}}^{1.5}$, see e.g. Rivin (2002, Theorem 4). □

Proof of Proposition 2. By Theorem 2 and $n_{\boldsymbol{L}} \geq n_{\boldsymbol{Q}}$, we have $Cost(SLA) \geq \mathcal{O}(n_{\boldsymbol{Q}}^2/M)$. By Assumption 1 and $M = 1 + p$ it follows $Cost(SLA) \geq \mathcal{O}(N^2/p)$. To conclude note that $\bar{n} = 2N/p$. □

Proof of Proposition 3. Let $\boldsymbol{\theta}$ be an arbitrary permutation of $(a^{(0)}, a_1^{(1)}, \dots, a_{I_1}^{(1)}, a_1^{(2)}, \dots, a_{I_2}^{(2)})$ and denote by ℓ the position of $a^{(0)}$ in $\boldsymbol{\theta}$. To prove part (a) we show that, whenever $\ell < 1 + I_1 + I_2$, switching the positions of $a^{(0)}$ and the variables after it in $\boldsymbol{\theta}$ does not increase $n_{\boldsymbol{L}}$. Such switching of positions does not change the future set of θ_m for any $m \notin \{\ell, \ell+1\}$ and thus leaves also $n_{\boldsymbol{L},m}$ unchanged by its definition in (16). Moreover, since $a^{(0)}$ is connected to all other variables in $G_{\boldsymbol{Q}}$, it follows that $n_{\boldsymbol{L},m}$ equals the maximum value of $M-m+1$ for all θ_m located after $a^{(0)}$ in $\boldsymbol{\theta}$. Thus, when $a^{(0)}$ is in position ℓ both $n_{\boldsymbol{L},\ell}$ and $n_{\boldsymbol{L},\ell+1}$ take their maximal values and moving $a^{(0)}$ to position $\ell+1$ cannot increase the value of $(n_{\boldsymbol{L},\ell} + n_{\boldsymbol{L},\ell+1})$.

Assume now the ordering $(a^{(1)}_1, \dots, a^{(1)}_{I_1}, a^{(2)}_1, \dots, a^{(2)}_{I_2}, a^{(0)})$ for $\boldsymbol{\theta}$. By definition, $n_{\boldsymbol{L}} = \sum_{m=1}^{I_1+I_2+1} n_{\boldsymbol{L},m}$, $n_{22} = \sum_{m=I_1+1}^{I_1+I_2} n_{\boldsymbol{L},m}$ and $n_{\boldsymbol{L},M} = 1$, so to show part (b) of the theorem we need to prove $\sum_{m=1}^{I_1} n_{\boldsymbol{L},m} = \mathcal{O}(n_{\boldsymbol{Q}})$. Denote the number of non-zero entries in the m-th row of $\boldsymbol{Q}$ by $n_{\boldsymbol{Q},m}$, so that $n_{\boldsymbol{Q}} = \sum_{m=1}^{M} n_{\boldsymbol{Q},m}$. By construction, $a^{(0)}$ is connected to all other variables in $G_{\boldsymbol{Q}}$ while the rest of $G_{\boldsymbol{Q}}$ bipartite into the $\boldsymbol{a}^{(1)}$ and $\boldsymbol{a}^{(2)}$ block, which imply $\sum_{m=1}^{I_1} n_{\boldsymbol{Q},m} = \sum_{m=I_1+1}^{I_1+I_2} n_{\boldsymbol{Q},m} = \mathcal{O}(n_{\boldsymbol{Q}})$. The absence of edges among elements of $\boldsymbol{a}^{(1)}$ in $G_{\boldsymbol{Q}}$ also implies that $n_{\boldsymbol{L},m} = n_{\boldsymbol{Q},m}$ for $m = 1, \dots, I_1$. We thus have $\sum_{m=1}^{I_1} n_{\boldsymbol{L},m} = \sum_{m=1}^{I_1} n_{\boldsymbol{Q},m} = \mathcal{O}(n_{\boldsymbol{Q}})$ as desired. □

Proof of Proposition 4. We prove $n_{\boldsymbol{L},m} \leq c\bar{n}$ for all $m = 1, \dots, 2I+1$, for some constant c independent of N and d. The latter implies $n_{\boldsymbol{L}} = \sum_{m=1}^{2I+1} n_{\boldsymbol{L},m} \leq c(2I+1)\bar{n} = \mathcal{O}(\bar{n}I)$. Direct computation of the non-zero entries in $\boldsymbol{Q}$ shows $n_{\boldsymbol{Q}} = 1 + 6I + 2\bar{n}I = \mathcal{O}(\bar{n}I)$, which thus implies that $n_{\boldsymbol{L}}/n_{\boldsymbol{Q}}$ is uniformly upper bounded. Also, $n_{\boldsymbol{L},m} \leq c\bar{n}$ implies $Cost(SLA) = \mathcal{O}(\sum_{m=1}^{2I+1} n^2_{\boldsymbol{L},m}) \leq \mathcal{O}(I\bar{n}^2) = \mathcal{O}(N\bar{n})$.

First we prove $n_{\boldsymbol{L},m} \leq 2\bar{n}$ for all $m = 1, \dots, 2I+1$. The circulant design assumption, namely $n^{(1,2)}_{ij} = 1$ when $|i-j| \leq d/2 \mod I$ and zero otherwise, implies $\bar{n} = \sum_{j=1}^{I} n^{(1,2)}_{ij} = \sum_{i=1}^{I} n^{(1,2)}_{ij} = d+1 \geq 3$ for every i and j. As shown in the proof of Proposition 3, we have $n_{\boldsymbol{L},m} = n_{\boldsymbol{Q},m}$ for $m = 1, \dots, I$, which in this case implies $n_{\boldsymbol{L},m} = 2 + \bar{n} \leq 2\bar{n}$. Again by the circulant design assumption we have that for $m = I+1, \dots, 2I$

$$\{j \geq m \,:\, \text{the future set of } \boldsymbol{\theta}_m \text{ does not separate it from } \boldsymbol{\theta}_j \text{ in } G_{\boldsymbol{Q}}\} \subseteq \tag{37}$$
$$\{m, m+1, \dots, m+d, 2I-d+1, 2I-d, \dots, 2I, 2I+1\}\,, \tag{38}$$

which by (16) implies $n_{\boldsymbol{L},m} \leq 2(d+1) = 2\bar{n}$. Finally we have $n_{\boldsymbol{L},m} = 1$ for $m = 2I+1$ again by (16). Thus we have $n_{\boldsymbol{L},m} \leq 2\bar{n}$ for all $m = 1, \dots, 2I+1$. The latter implies $n_{\boldsymbol{L}} = \sum_{m=1}^{2I+1} n_{\boldsymbol{L},m} \leq 2\bar{n}(2I+1) = \mathcal{O}(\bar{n}I)$. By definition of crossed design models and by the balanced levels condition, we also have $n_{\boldsymbol{Q},m} = 2 + \bar{n}$ for $m = 1, \dots, 2I$ and $n_{\boldsymbol{Q},m} = 1+2I$ for $m = 2I+1$, which imply $n_{\boldsymbol{Q}} = \sum_{m=1}^{2I+1} n_{\boldsymbol{Q},m} = 1+6I+2\bar{n}I = \mathcal{O}(\bar{n}I)$. Combining the above expressions we obtain that $n_{\boldsymbol{L}}/n_{\boldsymbol{Q}} \leq (\bar{n}(2I+1))/(\bar{n}I+3I) \leq 3$, thus implying that $n_{\boldsymbol{L}}/n_{\boldsymbol{Q}}$ is uniformly upper bounded with respect to N and d. Finally, $n_{\boldsymbol{L},m} \leq 2\bar{n}$ for all m, implies that $Cost(SLA) = \mathcal{O}(\sum_{m=1}^{2I+1} n^2_{\boldsymbol{L},m}) \leq 4(2I+1)\bar{n}^2 = \mathcal{O}(I\bar{n}^2) = \mathcal{O}(N\bar{n})$. Since $n_{\boldsymbol{L},m} = 2 + \bar{n}$ for $m = 1, \dots, I$ then one also has $Cost(SLA) = \mathcal{O}(\sum_{m=1}^{2I+1} n^2_{\boldsymbol{L},m}) \geq I\bar{n}^2 = \mathcal{O}(N\bar{n})$, thus proving $Cost(SLA) = \mathcal{O}(N\bar{n})$ as desired. □

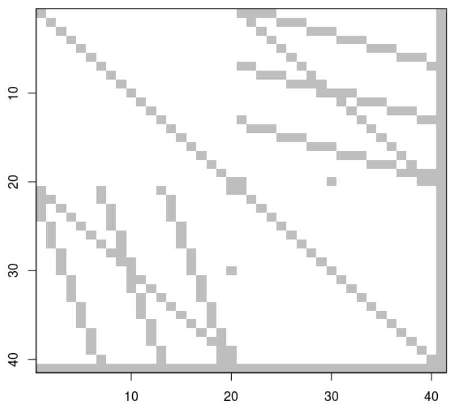

Figure 9.: Precision matrix $\boldsymbol{Q}$ of $\mathcal{L}(\boldsymbol{\theta} \mid \boldsymbol{y}, \boldsymbol{\gamma})$ induced by the worst-case balanced level design with $I = 20$, $d = 3$ and default ordering $(a_1^{(1)}, \ldots, a_I^{(1)}, a_1^{(2)}, \ldots, a_I^{(2)}, a^{(0)})$.

A.1. Worst-case balanced levels design for $Cost(SLA)$

Given a fixed integer $d \geq 2$, define a balanced level design with $\bar{n} = d + 1$ as follows: for $i = 1, \ldots, I-1$, set $n_{ij}^{(1,2)} = 1$ if at least one of the following conditions hold:
(a) $i = j$
(b) $d(i-1) \leq j - 2 < di \mod (I-1)$ and $i < j$
(c) $d(i-1) \leq j - 1 < di \mod (I-1)$ and $i > j$
and $n_{ij}^{(1,2)} = 0$ otherwise; while for $i = I$ set $n_{ij}^{(1,2)} = 1$ if $\sum_{i=1}^{I-1} n_{ij}^{(1,2)} \leq d$ and $n_{ij}^{(1,2)} = 0$ otherwise. See Figure 9 for an illustration of the resulting precision matrix $\boldsymbol{Q}$ when $I = 20$ and $d = 3$. It can be verified that the resulting design satisfies the balanced levels.

Lemma 1. *The resulting design satisfies the balanced levels condition with $\bar{n} = 1 + d$.*

Lemma 1 is easy to verify case by case, but its general proof is tedious and we omit it here for brevity.

Proposition 5. *Under the design defined above with d fixed and $I \to \infty$, it holds that $n_{\boldsymbol{Q}} = \mathcal{O}(p\bar{n})$, $n_{\boldsymbol{L}} = \mathcal{O}(p^2)$. Also, $Cost(SLA) = \mathcal{O}(p^3)$ while $Cost(Gibbs) \leq \mathcal{O}(p\bar{n}^2)$. All the constants are independent of N and d.*

Proof of Proposition 5. Define the function $r : \{1, \ldots, I\} \mapsto \{1, \ldots, I\}$ as $r(1) = 1$ and $r(j) = \lceil d^{-1}(j-1) \rceil$ for $j = 2, \ldots, I$, so that $n_{r(j)j}^{(1,2)} = 1$ for all $j \geq 1$. Then, for every couple j and m such that $r(j) \leq m \leq j$ we now show that the future set of $a_m^{(2)}$ does not separate it from $a_j^{(2)}$ in $G_{\boldsymbol{Q}}$. We construct a path in $G_{\boldsymbol{Q}}$ between $a_m^{(2)}$ and $a_j^{(2)}$ that goes through $a_1^{(2)}$ as follows. Since both $n_{jj}^{(1,2)}$ and $n_{r(j)j}^{(1,2)}$ are positive for all $j \geq 1$, the path going from $a_j^{(2)}$ to $a_{r(j)}^{(1)}$ to $a_{r(j)}^{(2)}$ to $a_{r(r(j))}^{(1)}$ to $a_{r(r(j))}^{(2)}$ etc. is supported on $G_{\boldsymbol{Q}}$. Also, since $r(\ell) < \ell$ for all $\ell \geq 2$ and $r(1) = 1$, the above path eventually reaches $a_1^{(2)}$. The same strategy can be applied to construct a path in $G_{\boldsymbol{Q}}$ from $a_m^{(2)}$ to $a_1^{(2)}$. Joining the two above paths at $a_1^{(2)}$, we obtain a path from $a_m^{(2)}$ to $a_j^{(2)}$ in $G_{\boldsymbol{Q}}$. The assumption $r(j) \leq m \leq j$ together with $r(\ell) \leq \ell$ for all ℓ ensures that such path does not involve elements in the future set of $a_m^{(2)}$ apart from $a_j^{(2)}$. Thus, by (16), $\boldsymbol{L}[a_j^{(2)}, a_m^{(2)}]$ is a potential non-zero whenever $r(j) \leq m \leq j$, meaning that the row of $\boldsymbol{L}$ corresponding to $a_j^{(2)}$ contains at least $j - r(j) + 1$ potential non-zeros. Summing over j we obtain

$$n_{\boldsymbol{L}} \geq \sum_{j=2}^{I}(j - r(j) + 1) \geq \sum_{j=2}^{I}(j - \frac{j-1}{d}) \geq \frac{d-1}{d}\sum_{j=2}^{I} j = \frac{d-1}{d}\left(\frac{I(I+1)}{2} - 1\right).$$

Thus $n_{\boldsymbol{L}} = \mathcal{O}(I^2)$ which also implies $Cost(SLA) = \mathcal{O}(I^3)$ by the lower bound in Theorem 2. The statements about $n_{\boldsymbol{L}}$ and $Cost(SLA)$ follow from the above equalities and $p = 1 + 2I$. The statement about $Cost(Gibbs)$ follows directly from Theorem 1, $N = I\bar{n}$ and the fact that the design has balanced levels. $\square$

B. Details on methodology

B.1. Second order update sampler for $L = 1$

For $L = 1$, we update $\mathcal{L}(\xi_i^{(k)} \mid \boldsymbol{y}, \boldsymbol{\gamma}, \boldsymbol{a}^{(-k)})$ by expanding it to second order. This results in the proposal law $\mathcal{N}(m_i^{(k)}(\xi_i^{(k)}), c_i^{(k)}(\xi_i^{(k)}))$, where

$$m_i^{(k)}(\xi_i^{(k)}) = c_i^{(k)}(\xi_i^{(k)})\left(\partial f_i^{(k)}(\xi_i^{(k)} - a^{(0)}) + \tau_k a^{(0)} - \partial^2 f_i^{(k)}(\xi_i^k - a^{(0)})\xi_i^k\right),$$
$$c_i^{(k)}(\xi_i^{(k)}) = \left(\tau_k - \partial^2 f_i^{(k)}(\xi_i^{(k)} - a^{(0)})\right)^{-1}.$$

and $m_i^{(k)}$ corresponds to the Newton-Raphson update. A proposal $\tilde{\xi}_i^{(k)}$ is accepted with probability

$$1 \wedge \frac{f_i^{(k)}(\tilde{\xi}_i^{(k)} - a^{(0)})\,\mathcal{N}(\tilde{\xi}_i^{(k)}; a^{(0)}, \tau_k^{-1})\,\mathcal{N}(\xi_i^{(k)}; m_i^{(k)}(\tilde{\xi}_i^{(k)}), c_i^{(k)}(\tilde{\xi}_i^{(k)}))}{f_i^{(k)}(\xi_i^{(k)} - a^{(0)})\,\mathcal{N}(\xi_i^{(k)}; a^{(0)}, \tau_k^{-1})\,\mathcal{N}(\tilde{\xi}_i^{(k)}; m_i^{(k)}(\xi_i^{(k)}), c_i^{(k)}(\xi_i^{(k)}))}. \tag{39}$$

B.2. Acceptance probability of gradient-based sampler

For $L > 1$, we propose an update to $\mathcal{L}(\boldsymbol{\xi}_i^{(k)} \mid \boldsymbol{y}, \boldsymbol{\gamma}, \boldsymbol{a}^{(-k)})$ from $\mathcal{N}(\boldsymbol{m}_i^{(k)}(\boldsymbol{\xi}_i^{(k)}), \boldsymbol{D}_i^{(k)})$, where

$$\boldsymbol{m}_i^{(k)}(\boldsymbol{\xi}_i^{(k)}) = \boldsymbol{C}_i^{(k)}\left(\boldsymbol{\xi}_i^{(k)}/\delta_i^{(k)} + \nabla f_i^{(k)}(\boldsymbol{\xi}_i^{(k)} - \boldsymbol{a}^{(0)}) + \boldsymbol{T}_k \boldsymbol{a}^{(0)}\right),$$
$$\boldsymbol{D}_i^{(k)} = \boldsymbol{C}_i^{(k)} + \left(\boldsymbol{C}_i^{(k)}\right)^2/\delta_i^{(k)}, \quad \boldsymbol{C}_i^{(k)} = \left(\boldsymbol{T}_k + \boldsymbol{I}/\delta_i^{(k)}\right)^{-1}.$$

A proposal $\tilde{\boldsymbol{\xi}}_i^{(k)}$ is accepted with probability

$$1 \wedge \frac{f_i^{(k)}(\tilde{\boldsymbol{\xi}}_i^{(k)} - \boldsymbol{a}^{(0)})\,\mathcal{N}(\tilde{\boldsymbol{\xi}}_i^{(k)}; \boldsymbol{a}^{(0)}, \boldsymbol{T}_k^{-1})\,\mathcal{N}(\boldsymbol{\xi}_i^{(k)}; \boldsymbol{m}_i^{(k)}(\tilde{\boldsymbol{\xi}}_i^{(k)}), \boldsymbol{D}_i^{(k)})}{f_i^{(k)}(\boldsymbol{\xi}_i^{(k)} - \boldsymbol{a}^{(0)})\,\mathcal{N}(\boldsymbol{\xi}_i^{(k)}; \boldsymbol{a}^{(0)}, \boldsymbol{T}_k^{-1})\,\mathcal{N}(\tilde{\boldsymbol{\xi}}_i^{(k)}; \boldsymbol{m}_i^{(k)}(\boldsymbol{\xi}_i^{(k)}), \boldsymbol{D}_i^{(k)})}. \tag{40}$$

Notice that the matrices $\boldsymbol{D}_{i_1}^{(k)}, \dots, \boldsymbol{D}_{I_k}^{(k)}$ all share the same eigenspace. Accordingly, an efficient implementation of the update first eigendecomposes $\boldsymbol{T}_k = \boldsymbol{V}\boldsymbol{\Lambda}\boldsymbol{V}^T$, where $\boldsymbol{\Lambda}$ is diagonal and invertible in $\mathcal{O}(L)$ time, then computes

$$\left(\boldsymbol{D}_i^{(k)}\right)^{1/2} = \boldsymbol{V}\left((\boldsymbol{\Lambda} + \boldsymbol{I}/\delta_i^{(k)})^{-2}/\delta_i^{(k)} + (\boldsymbol{\Lambda} + \boldsymbol{I}/\delta_i^{(k)})^{-1}\right)^{1/2}.$$

We proceed to use the square root to simulate the proposal and to evaluate its density.

C. Details on numerics

C.1. Priors

The crossed effects multinomial logit model introduces the complication of being ill-identified due to softmax being invariant under translations of $\boldsymbol{\eta}_j$. While it is identified a posteriori under the symmetrical Wishart prior, the development of efficient algorithms for the symmetrical model is beyond the scope of this paper. Instead, we follow the common practice of fixing the coefficients pertaining to the L-th response:

$$a_{iL}^{(k)} = 0, \quad i = 1, \dots, i_k, \quad k = 0, \dots, K. \tag{41}$$

The priors on $\boldsymbol{a}^{(0)}$ and $\boldsymbol{a}^{(k)}$ follow from the general model in (1) by setting $\boldsymbol{T}_{pr}^{-1} = \boldsymbol{I}$. This fairly informative prior aids in identifying $\boldsymbol{a}^{(0)}$ more firmly. We set proper, weakly informative Wishart priors on all elements of $\boldsymbol{\gamma}$, which corresponds to (3) with hyperparemter $L-1$. In summary, in the election crossed effect model we have:

$$K = 7,\ I = \sum_{k=1}^{7} I_k = 70,\ L = 3, N \approx 10^4, p = 140 \tag{42}$$

and the ratio of cells in the contigency table with observations is approximately 15%.

For the nested model, priors on $\boldsymbol{\beta}_{i_1 \dots i_k}$ follow from the general model in Section 1.3 and (5) by setting $\boldsymbol{\Sigma}_{i_1 \dots i_k} = \boldsymbol{\Sigma}_k$ and $\boldsymbol{A}_{i_1 \dots i_k} = \boldsymbol{I}$ and on $\boldsymbol{\beta}_0$ by setting $\boldsymbol{T}_{pr}^{-1} = \boldsymbol{0}\boldsymbol{0}^T$. We set proper, weakly informative inverse Wishart priors on all elements of $\boldsymbol{\gamma}$, which corresponds to setting the hyperparameter to L. The residual variance parameters are assumed to be independent a priori, with distribution

$$\mathcal{L}(2\phi_{i_1 \dots i_K}^2) = \mathcal{IG}(1/2, 1/2), \qquad i_K = 1, \dots, I_K. \tag{43}$$

In summary, in the real estate prices nested multilevel model we have:

$$K = 4,\ I_1 = 52,\ I_2 = 375,\ I_3 = 1448,\ I_4 = 2136,\ L = 2, N \approx 4 \times 10^6, p \approx 8 \times 10^3 \tag{44}$$

and the fraction of non-zero elements in $\boldsymbol{Q}$ is of the order 10^{-4}.

C.2. MCMC performance metrics

The *integrated autocorrelation time* (IAT), is defined as

$$\operatorname{iat} X = 1 + 2\sum_{t=1}^{\infty} \operatorname{acf}_t X \tag{45}$$

where X is a stochastic process and $\operatorname{acf}_t X$ is the autocorrelation function (ACF) of X evaluated at t-th lag. In practice, we estimate ACF by empirical averages from a single trajectory of X. We then use these estimates to estimate the IAT following Sokal's windowing heuristic Sokal (1997). The heuristic consists of computing a running sum over ACF lags and stopping as soon as the running sum exceeds a multiple of the next lag. We modify this heuristic slightly and only truncate at even lags to account for NUTS' tendency to produce estimates of ACF of different sign at successive lags. We define the *effective sample size* (ESS) as the run length divided by the IAT estimate. Since we are comparing methods with vastly different computing time per iteration, we monitor the run time of the algorithm for both algorithms and use *effective sample size per second* as our performance metric. Notice that we include transience time in the ESS/sec estimate. Moreover, when overlaying ACFs for both methods, we plot them as a function of computing time, as opposed to iteration lag.

C.3. VB performance metrics

We monitor absolute estimation error for posterior means and posterior log standard deviations at regular time intervals $(t_1, t_2, \dots, t^*)$. For ADVI, we obtain incremental estimates by stopping the optimization at $t_1, t_2, \dots$ and generating samples from the current approximation. For SLA/cGibbs, we start the algorithm from the variational approximation at time 0, run it up to t^* and produce estimates from the parts of the chain generated in the time intervals $(t_1/2, t_1), (t_2/2, t_2), \dots$. Removing the first half of the interval improves estimates because the Gibbs sampler for non-Gaussian likelihoods typically doesn't reach stationarity until t^* due to the adaptation of its tuning parameters. The total length t^* is chosen to coincide with convergence of ADVI.

C.4. Simulation settings for Section 6

For the comparisons between VB and our MCMC, we obtain the ground truth by a run of length 100000 of our MCMC method (SLA-based or collapsed Gibbs sampler), with an additional adaptation period for the adaptive collapsed Gibbs sampler.

We plot ACF as a function of *iteration time*, which is defined as the wall time of the full run (including adaptation) divided by the number of sampling iterations (excluding adaptation), hence the actual time needed to collect useful samples is reflected in the figures.

C.5. Figure 4

$Cost(SLA)$ is obtained according to the equality in Theorem 2 but with the explicit constants as laid out in the proof of the Theorem. $Cost(Gibbs)$ is computed by multiplying $n_{\boldsymbol{Q}}$, which corresponds to cost per iteration, by the relaxation time of the Gibbs sampler. The relaxation time for these models is calculable, even if not available in closed form, in terms of the largest absolute eigenvalue of an explicit matrix, as exposed in Theorem 1 of Roberts and Sahu (1997).